NTNU

Norwegian University of
Science and Technology

In-transit cargo transfer between ships

Aleksander Vladimirovitsj Veksler

Master of Science in Engineering Cybernetics
Submission date: June 2009
Supervisor: Alexey Pavlov, ITK

Norwegian University of Science and Technology
Department of Engineering Cybernetics

Problem Description

In several important applications there is a need to deliver large equipment from heavy transport ships onto shores that do not have seaports and are not easily accessible by land. One possible solution to this problem is based on reloading the equipment from the transport ships onto smaller crafts capable of delivering the equipment onshore.

The Cymer Center for Control Systems and Dynamics at UCSD is exploring the concept of employing a ramp between the two vessels for this problem. The main difficulty in safely transporting equipment between two ships is due to the waves. To counteract the effect of the waves, an active ramp system needs to be designed.

The task of this thesis is explore the concept of an active ramp between the ships. The system can include active control of the ships for their synchronization and compensation of the wave effect. The design goal is to minimize the wave-induced motion of the ramp. The student is free to choose between a configuration with ships being placed side-to-side or bow-to-stern, and to decide where and how it is feasible to place the actuators. The design should be supported analytically and verified in simulations.

Assignment given: 01. November 2008
Supervisor: Alexey Pavlov, ITK

Contents

List of Figures

List of Tables

Abstract

Cargo transfer between two vessels at sea requires the ramp connection between the vessels to be as stable as possible. The complex nature of the system makes employing control methods difficult. This thesis explores two ideas for improving performance of the interconnected system.

First idea examines the possibility of actuating the smaller of the vessels with fins, so as to reduce the relative movement between the two points where the ramp is connected to the ships.

The second idea using the larger ship to shield the smaller one from incoming waves. It is assumed that the total disturbance is minimized at a certain angle to the waves, and an Extremum-Seeking based controller is used to find this angle. To allow ship models to change dynamically as cargo offloads, the technique of extremum seeking is extended in this thesis to allow a certain type of model uncertainties.

Assignment Text

In several important applications there is a need to deliver large equipment from heavy transport ships onto shores that do not have seaports and are not easily accessible by land. One possible solution to this problem is based on reloading the equipment from the transport ships onto smaller crafts capable of delivering the equipment onshore.

The Cymer Center for Control Systems and Dynamics at UCSD is exploring the concept of employing a ramp between the two vessels for this problem. The main difficulty in safely transporting equipment between two ships is due to the waves. To counteract the effect of the waves, an active ramp system needs to be designed.

The task of this thesis is explore the concept of an active ramp between the ships. The system can include active control of the ships for their synchronization and compensation of the wave effect. The design goal is to minimize the wave-induced motion of the ramp. The student is free to choose between a configuration with ships being placed side-to-side or bow-to-stern, and to decide where and how it is feasible to place the actuators. The design should be supported analytically and verified in simulations.

Acknowledgements

I did most of the work on this thesis on exchange at University of California, San Diego. I would like to thank Professor Miroslav Krsti¸ of UCSD for being my supervisor on this project, and high-quality scientific guidance he provided. I would also like to thank Professor Alexey Pavlov of NTNU for always being there when I needed him, despite the distance. The other students in my project group, Joe Doblack and Jacob Toubi, have consistently contributed with day-to-day research, as well as helping me understand the American culture. Further, I would like to give special thanks to my family, Rosa and Edgar Kristiansen.

This document was written in LyX

Chapter 1

Introduction

The transfer of cargo over a ramp from a LMSR (large, medium-speed, roll-on/roll-off) vessel to a connector vessel in high sea states represents significant challenges for ship and control system designers. This thesis is part of a project the goal of which is to ultimately determine the actuation/sensing requirements and to devise control and real-time optimization algorithms for reducing the oscillations of the pitch, roll, and yaw angles between the ramp and each vessel.

The system investigated consists of a Sea Base (the large vessel) and a T-Craft (the connector vessel) connected by a ramp that can vary in length. Designs with ships placed side-by-side and aft-to-fore are considered. Due to the number of degrees of freedom involved in this system, deriving the equations of motion is challenging, even when the hydrodynamic force laws are known. For this reason, limiting the complexity of the model down to what is strictly necessary to achieve a particular design goal is an important part of this work.

The study group working on this project consists of three students in addition to myself and were headed directly by Professor Miroslav Krstić. Several strategies for compensating for the wave motion were considered at the time the present author joined the project in the end of September 2008.

One proposal that was an extention mechanism on the ramp that would allow it to change length dynamically, although not fast enough to be effective on wave frequencies. Another proposal was to set up variable dampeners and/or springs with variable constant at connection points between the ships and the ramp. Orientation of the ships relative to wave fronts was also experimented with. Given that the disturbance caused by the waves has its minimum for a certain length of the ramp, for a certain damping and for a certain spring constant and for a certain orientation into the wave front according to some representative performance criterion, Extremum Seeking technique can be used to keep those controlled parameters at their optimal values. The simulations were carried out in a Matlab package called SimMechanics, which allows simulation of mechanical systems by specifying components such as springs, rigid connections, joints etc. However, none of the solutions were close to maturity at the time this author joined the project, and there was need to increase the breadth of the work by exploring additional concepts.

In this thesis, the decision was made to explore two different approaches. The first approach that was considered, was adding two sets of fins in front and in the back of the smaller vehicle in aft-to-fore configuration. This allows creating force in heave (for the smaller vehicle), as well as a torque in pitch. Theoretically this also allows creating a torque in roll, but because of the way the ramp is connected this would only serve to break the ramp. This approach is the one used for illustration on the front page of this thesis. After some consideration, only pitch of the smaller vehicle was put under control, attempting to hold the angle of the ramp as small as possible. The control task for this part turned out to be very simple, with an LQR controller doing the job adequately.

The second approach considered in this work is used for side-to-side configuration and exploits the fact that ships have different sizes. This means that the smaller ship is more affected by the waves, and it makes sence for the larger ship to shield it. Maximal shielding is attained when the ships are turning their sides towards the wave front with the large ship shielding the small one from the waves. However, most ship designes are far less affected by the waves when sailing into the wave fronts. This means that the ships should sail into the waves on an angle which is optimal according to some performance criterion. Extremum Seeking technique is to be used to find this optimal angle. To some extend this overlaps work of the other team members. However, while the work done by the other team members focuses on simultaneus regulation of orientation, spring constants and ramp length in a SimMechanics model, this work uses only a very simple model for the ship dynamics in yaw and focuses on compensating for changes in the weight of the ships through the transfer. This involves an extension of Extremum Seeking was necessary to allow it to handle models that exprience a priori unknown variations in time.

In the begining of the project, an extensive attempt was made to find similar solutions through relevant professional publications, which was not successfull. Neither were such solutions known to the client of this project. [5] contains useful results on ships equiped with fins for different purposes, and those results are extensively used here. As to probing frequency phase lag tracking which will be presented in Chapter 4, no similar extention was attempted in the litterature before before.

This thesis is a part of a large, ongoing project early in its developement. The goal of this thesis is limited to concept exploration, and the it does not intend to present a complete solution for the task in hand.

The system is described in more detail in chapter two. The concept of controlling the smaller ship with fins is explored in Chapter 3, and Chapter 4explores the idea of shielding the smaller ship by positioning the larger ship between it and the incoming waves, controlled by an extremum-seeking controller with extension mentioned above.

Chapter 2

General Description of the System

Since the project was already well underway when this author joined the team, some space needs to be devoted to introduce the reader to the project, the assumptions made as well as the solutions considered.

To transport equipment between the vessels, a ramp is proposed to be extended between them. In the beginning of the project, little was known about the expected sizes of the ships, weight and tolerance limits of the ramp and the system to be used to attach it to the vessels. It became known later that the smaller ship (the T-craft) is likely to be a Surface Effect Ship (SES).

As is usual in engineering, when something is not known, reasonable working assumptions have to be made temporarily in order to allow the project to continue until the assumptions may be replaced with real data. Some of the assumptions were decided by the project leader, while others were made by this author.

Following assumptions are part of given specifications:

1. The ramp has a flexibility to rotate up and down on attachment points, but the attachment point itself does not move.
2. The length of the ramp can not be changed on wave frequency.

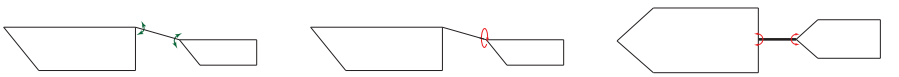

(a) "Up-and-down" movements OK

(b) One ship can not rotate in roll without the other also rotating

(c) The two ships have to have the same heading

Figure 2.1: Illustration of how the ramp limits the degrees of freedom of the ships

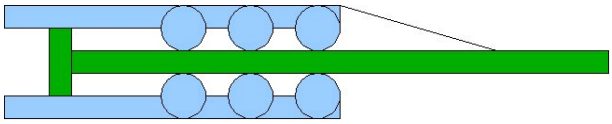

Figure 2.2: Joint for a passively extendable ramp. Instead of having a mechanism on the ramp that extends it to a given length, the proposed ramp has flexible length. The length may be set by positioning of the ships. The T-shaped green part is free to move sideways inside the blue part. Equipment can be moved on top.

3. The length of the ramp were to be controlled by an unspecified mechanism on the ramp, but not fast enough to have significant effect on wave frequencies.

4. It is preferred that the stabilization of the ramp is achieved by steering the T-craft.

5. The ramp is infinitely strong, constraining the distance between the points where it is attached to a constant. In 3-dimensional case, the ramp will also keep the ships on a straight line (seen from above).

In addition, for the system where the ramp is attached at the bow of one of the ships and stern of the other (*bow-to-stern configuration*), the ramp is assumed to be strong enough to keep the ships on the same orientation in roll. An interesting simplification can be made as a consequence of this assumption. Decomposing the wave action into lateral and head-on forces, it is apparent that that lateral wave forces only affect roll and sway, as well as yaw of the system as a whole without changing relative positions of the bodies in this three-body system. While roll can cause significant problems for cargo transfer, research into roll stabilization of ships is already at a very mature state and several practical solutions are mentioned in [5] and are directly applicable here because the ramp essentially forces the two vessels to behave as a rigid body in roll. For stabilization of the ramp in heave and in pitch, *a two-dimensional model is sufficient.*

This author also proposed a system with passively extendable (i.e. flexible) ramp as desribed in Figure 2.2. Results from [9] or [10] could be used to keep the two ships on a specified distance, implicitly controlling the ramp length without any additional machinery. The design was however rejected. Another design that was discussed was a connection that would allow the ramp full flexibility to rotate on attachment points.

Chapter 3

Fin Stabilization

In this chapter, the ability to actuate the smaller vessel with fins in the pitch DOF to reduce the roll of the ramp[1] will be considered. A simplified version of the system is simulated, and an estimate for the necessary size of the fins is provided. Because few people familiar with control theory are also familiar with aerodynamics, the first section is short introduction to foil theory.

The contents of this chapter are practically oriented. Fin stabilization of an interconnected ship system is a novel idea, and this work makes no attempt to bring it beyond the conceptual stage. A significant effort has gone into keeping the model mathematically simple, in order to concentrate on understanding of the general properties of the system.

3.1 Key concepts in foil theory and application to hydrofoils

In this section, basic concepts from hydrodynamics are introduced. This introduction by no means intends to be exhaustive. Many good books are written on the subject, and this introduction does not. [4] comes highly recommended, and [5] pages 178-205 also covers quite well, but reading it without prior knowledge may prove to be a formidable challenge. [3] is excellent for general reference, [7] provides a quick and very interesting introduction (more detailed than the presentation in this chapter but less complicated than the presentation in [4]).

A hydrofoil is a device designed to operate in a flow of water in such a way as to produce maximal force tangential to the flow (lift), while keeping the force parallel to the flow direction (drag) as low as possible. Both water and air are considered incompressible and inviscid in a wide range of engineering applications. Indeed, subsonic flows where compressibility effects are insignificant are *similar* in water and in air for the same Reynold's number. It is therefore not

[1] The way coordinates for the ramp are defined in this project, the ramp orientation is "perpendicular" on the ships. For example, when one of the ships lifts in heave, the ramp *rolls,* not pitches.

Figure 3.2: Kutta-Zhukovsky explanation of the generation of lift by adding large scale circulation to potential flow

surprising that both [5], a book about marine applications, and [4], a book about aerodynamics, use potential theory to approximate lifting force of a foil[2], and theory from the two books is used in this thesis interchangably. This introduction is meant as a very superficial background for the material in this chapter. The reader is also assumed to have basic knowledge of fluid dynamics, such as potential and stream functions, superposition of flows, basic flow patterns such as uniform flow, sources and sinks, doublets, and not least the vortex flow.

D´Alembert's paradox suggests that no force - neither lift nor drag - is exerted on a body in an incompressible and inviscid flow. This obviously contradicts empirical data. Indeed, potential theory, which is both limited to and fully describes incompressible and inviscid flow, predicts the flow pattern as shown on Figure 3.1. Since the trailing edge is (infinitely) sharp, the fluid has experiences (infinitely) high acceleration while rounding the edge, which leads to (infinitely) high viscocity and thus (infinitely) high viscous forces. To resolve this situation, the so-called *Kutta condition* is introduced, which postulates that at the trailing edge the fluid flowing from overside of the foil has exactly same velocity as the fluid flowing from underside of the foil. This can be achieved by modifying the potential field with vortices.

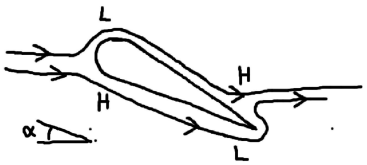

Figure 3.1: Potential flow around an airfoil. Air flows around the trailing edge of the foil, generating no lift as "predicted" by DÁlembert's paradox. A real flow, at least for any Reynold's number significantly above zero, the flow will detatch at the trailing edge, creating lift.

A single vortex is a fluid circulation around a single point, with circulation velocity expressed in polar coordinates $v_\theta = -\frac{\Gamma}{2\pi r}$, $v_r \equiv 0$, where Γ is the stength of the vortex. An interesting property of a vortex is that it generates lift proportional to the incoming uniform flow and the strength of the vortex. A rough drawing of the effect of a vortex on the potential field around a wing profile is shown on Figure 3.2. For a thin airfoil of infinite span at a small angle of attack, a good approximation of the lift (but not drag) can be achieved by placing a vortex sheet, which is a contiuous distribution of vortices.

When airfoil has a finite span, the fluid begins to move in spanwise direction, and not only along the chord. This flow is caused by pressure difference between

[2]But not the drag.

overside of the airfoil (where there normally is suction) and underside (where there normally is overpressure). This pressure spillage causes a wing of finite span to have a lower lift per unit length than a foil of ininite span. One way to limit this spilage is to employ wingtip devices such winglets. They to limit pressure spillage, but they also induce drag and they add to the weight of the wing so advantage of using them is less obvious than one can assume intuitively.

One way of modeling wing of finite span is by using vertices formed as horseshoes to form a lattice in such way as two give a good approximation of the flow around the wing. This approach is described in [4] page 260 and [5] page 184.

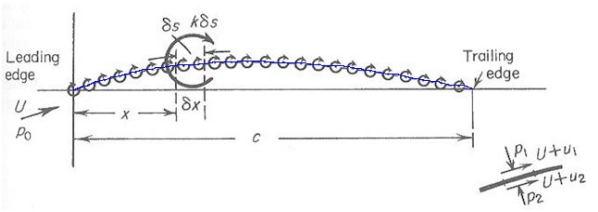

Figure 3.3: A vortex sheet. The airfoil is the blue line going through the centers of the ininitesimal vortices with strength $s = s(x)$, assumed to be thin and infinite in both directions perpendicular to the paper. The total strength Γ of the vortices is $\Gamma = \int_0^c s(x)dx$. The strength distribution of the vortices has to be such that flow *through* the airfoil is always zero, while satisfying the Kutta condition

Because of the pressure spillage, airfoils with high aspect ratio (i.e. "longer" wings) generate more lift per unit area and thus have better lift/drag ratio. For a sailplane, where lift/drag relationship is the decisive characteristic, wings with aspect ratio of up to 35 may be used, only limited by the structural strength of a wing at a given weight. On a fighter jet, the wing may experience significant stresses, it has to be optimized for trans- and supersonic flight as well as other considerations such as vibrations, place on deck of an aircraft carrier etc, and wings with aspect ratio as low as 2 are used.

To round off the this theoretical introduction it should be mentioned that the potential flow-based methods mentioned above have long since been replaced with more rigorous numerical formulations (199 in [4]). [7] goes as far as to calls the vortex placement method "mathematical fiction". However, vortex placement does provide a valuable intuitive insight into flows around a wing, and are still taught in indroductory aerodynamics classes.

The speed of sound in water is about 1550 m/s so no hydrofoil will be going transsonic in the near future and hydrofoils with high aspect ratio are prefered. However, because sea water is about 850 times denser than air, the lift of the same section is also greater, which puts a bigger strain on the structure of the foil. Because of this, as well as consideration to physical space at the sides of the vehicle, aerofoils with aspect ratio of about 5 are suggested.

3.2 Preliminary analysis

The goal of this chapter is to propose a device capable of reducing the disturbances on the ramp in addition to solutions proposed by the other members of

the team. In order to calculate what it is natural to estimate the forces required to move a ship in heave or in pitch.

The calculation of the restoring forces - both for heave and pitch displacement - presented here is based on the calculations in [6] section 3.2.3 and makes many of the same assumptions. The mathematical representation is simpler here, mainly because it does not need to concern itself with the concept of metacentric height. This is necessary in [6], because it also treats forces in roll, and the distance between center of gravity and center of buoyancy at rest is significant for that purpose. At least for this author simpler mathematical representation results in better understanding of the physical system, and thus better understanding of which simplifications can be made and which would result in critical details being lost.

Since the project is at conceptual stage, nothing more than a rough estimate is needed. Refering to Table 3.1, estimating the area of the cross-section between the water plane and the shape of the vessel simply as width of the ship multiplied by its length.

While this approach may appear overly rough - the ship is after all not rectangular - the reader must remember that the ship dimensions in Table 3.1 are a very rough approximations to begin with, and little precision is lost while the model is greatly simplified. There is also a communicational advantage: this approach avoids creating an impression that the this analysis is more precise than it really is.

In this estimation work, it is calculated how much force is needed to displace one of the ends of the ramp a distance of two meters up or down either by displacing the vessel in heave by pitching it around its center of buoyancy. Even though we are projecting for seastate 4 where largest waves are about 2.5 meters, putting two of those meters under control is a significant improvement. When the ramp is fully extended to 20 meters, a three meter rise in each of the ends would result in $asin\left(\frac{2}{20}\right) = 6^\circ$ change of its angle, while on fully contracted ramp the two meter rise gives a change of $asin\left(\frac{2}{10}\right) = 12^\circ$.

First, we calculate the force needed to keep the Seabase two meters above or below the equilibrium point in heave:

$$F_{sb} = LW \underbrace{z\rho_{sw} \cdot g}_{pressure} = 200m \cdot 30m \cdot 2m \cdot \rho_{sw} \cdot g \approx 60 \cdot 10^6 \cdot 2N \approx 121 \cdot MN \quad (3.1)$$

The numerical values are from Table 3.1. For the T-craft, the number is

$$F_{tc} \approx 40m \cdot 16m \cdot \rho_{cw} \cdot g \cdot 2m \approx 13 \cdot MN \quad (3.2)$$

So how large fins are needed to provide this forces at speed of 10 m/s? The kinematic viscousity of water $\nu_w \approx 1\frac{m^2}{s} \cdot 10^{-6}$, for air it is $\nu_a \approx 15\frac{m^2}{s} \cdot 10^{-6}$. This means that for same geometry, a flow in water will have same Reynold's number $Re = \frac{VD}{\nu}$ as a flow in air at velocity V fifteen times lower than velocity in the air. Thus, a flow in water at 10 m/s is similar to the flow in air at 150

Length of the larger ship (Seabase)	200 m
Width of the larger ship (Seabase)	30 m
Length of the smaller ship (T-craft)	40 m
Width of the smaller ship (T-craft)	16 m
Length of the ramp	10-20 m
Seastate	4
Wave height observed (according to Table 4.2 in [6])	1.25-2.5 m

Table 3.1: Rough approximations of numeric values for dimensions of the ships and environment

m/s, the latter being a typical value in aviation. Airspeed of 150 m/s is not transsonic with a very good margin, so compressibility effects are not significant here[4].

According to table 7.10 in [4], the maximal lift coefficient for a wing of aspect ratio of 6 is 1.2. Since lift coefficient is defined per

$$C_L = \frac{L}{\frac{1}{2}\rho v^2 A} \tag{3.3}$$

We have

$$1.2 = \frac{L}{\frac{1}{2}\rho_{sw} v^2 A} \tag{3.4}$$

Solving the above for A while substituting $\rho_{sw} = 1030\frac{kg}{m^3}$, $v = 10\frac{m}{s}$ and $L = 121MN$ for the seabase and $L = 13MN$ for the T-craft, results in $A = 1958m^2$ for the Seabase and $A = 210m^2$ for the T-craft. Even for the T-craft, four fins sized 3x18 meters would be needed, which is somewhat above the practical limitations.

Now considering pitch actuation. In order for a 40 meter long craft to lift its bow a distance of two meters, it has to be rotated at an anle of $atan\left(\frac{2}{20}\right) = 5.7°$.

Again a few more approximations are needed. When the ship is tilted in pitch, for small angles it can be approximated as deforming the profile of the ship as drawn in Figure 3.4b. In this approximation, every geometrical point is displaced vertically instead of a circular path around the rotation center. This geometrical appoximation is valid when the ship's length is large compared to its height, and tilting angle is small. The total moment of the gravity force is

$$\tau_g = \int \vec{g} \times \vec{r}_{old} dm \tag{3.5}$$

Since every mass element is displaced vertically, the cross product of displacement with the gravity force is zero, i.e. $\vec{g} \times \vec{r}_{new} = \vec{g} \times (\vec{r}_{old} + \Delta\vec{r}) = \vec{g} \times \vec{r}_{old}$. This means that only the buoyancy force has changed.

Now, we want to calculate the total moment created by the buoyancy force when the ship is displaced in pitch from its equilibrium position. We define L

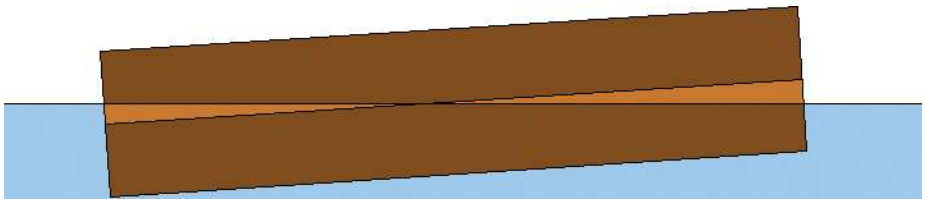

a: Tilted in pitch

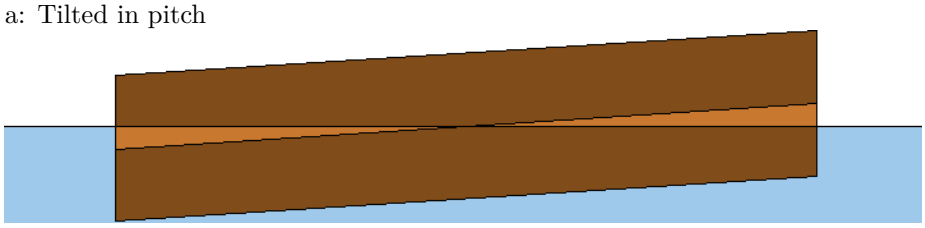

b: Parallelogram approximation

c: Parts entering and leaving water

Figure 3.4: Rotation around the center of buoyancy is approximated with paralellogram deformation.

to be the length of the ship and a coordinate system at the center of buoyancy. On most ships center of gravity will be placed under the center of buoyancy for additional stability. The arrangement could be thought of as ship's weight hanging on a thread as long as the difference between the center of buoyancy and center of gravity, with buoyancy force "holding" the thread (notice that if center of buoyancy is below the center of gravity, this force will make the ship more unstable). For torque in pitch however, this torque is completely dominated by the buoyancy force described here. We have

$$\tau_r = \int_{-\frac{L}{2}}^{+\frac{L}{2}} F(l) l \, dl \tag{3.6}$$

Where $F(l)$ is the force density of the restoring force per unit length along the ship (Newton/meter). To calculate $F(l)$ we can think of elements dl as independent columns going up and down from equilibrium positions. Setting up the force ballance on a body floating in water:

$$F + mg - \rho g V = 0 \tag{3.7}$$

Where V is the submerged volume. At equilibrium, $mg = \rho g V_0$, transforming the above to[3]

[3]A minor point that F in this equation is not per unit length.

$$F = \rho g(V - V_0) \tag{3.8}$$

For each element dl, the volume change compared to equilibrium position is

$$V - V_0 = \underbrace{l\,tan(\theta)}_{height}\,\underbrace{wdl}_{area} \tag{3.9}$$

Where θ is the current pitch angle. This allows tranformation of (3.6) to

$$\tau_r = \int_{-\frac{L}{2}}^{+\frac{L}{2}} \underbrace{\rho g l\,tan(\theta) W}_{F(l)}\, l\,dl \tag{3.10}$$

Solving the integral,

$$\tau_r = \rho g\,tan(\theta) W \left[\frac{l^3}{3}\right]_{-\frac{L}{2}}^{+\frac{L}{2}} = \rho g\,tan(\theta) W \frac{L^3}{12} \tag{3.11}$$

Now, placing two fins in front of the vehicle and two in the back and configuring them to create force pairs acting on the center of gravity with a torque $\vec{F}_f \times \vec{r} \approx F_f \cdot \frac{L}{2}$.This means that to create torue τ_r , a force

$$F_f = \tau_r / L \cdot 2 \tag{3.12}$$

is needed. Also, we can use $tan(\theta) = \frac{2}{0.5L}$. Substituting this into (3.11) yields

$$F_f = \rho g \cdot 2 \cdot W \frac{L}{3} \tag{3.13}$$

Thus, to keep the T-craft tilted on an angle of 5.7°, a total force of about $4.3MN$ is needed. The size of fins needed can be calculated using (3.4) to be $70m^2$. This can be provided with four fins 1.7m x 10m, which is completely practical. Indeed, comparing (3.1) and (3.13) shows that actuation in pitch is (roughly) three times more efficient than actuation in heave.

Why not do both heave and pitch? Consider the situation where the fins in front an in back are configured so as to create maximal torque in pitch. This means that they must create forces in opposite directions, ideally creating zero force in heave. If we want to create force in heave, either fins in the front or in the back have to turn away from this optimal position, cancelling some of the torque from the other set of fins. Since it is already established that actuation in pitch is more efficient, diverting effort to actuation is heave is suboptimal.

Thus, a practical estimate has been made with mininal information about the product in design. Although this result allows making the decision to proceed with the project and explore fin actuation further, this kind of modeling can also be dangerous if used without understanding it properly. The assumptions made throughout this section make the model very particular as to what to

result actually means. For example, the task assigned to fins was to keep the T-craft at a certain angle in pitch. This will never be the case because the T-craft will have to move so as to track the Seabase. Perhaps the waves will lift the two vessels together? Are waves large enough to disturb the operation of the fins? Will the fins create too much drag when operating with maximal lift, or is maximal lift only needed small percentage of the time? How will the fins interact with improvements proposed by the other members of the team? Could the fins be downsized and still provide a significant boost to performance of the system? The model in this section address none of those questions, and the engineer to design the system has to be aware that those problems exist when using this model[4].

3.2.1 Fin actuation in side-to-side configuration?

It is obvious that bow-to-stern configuraton is prefered when fin stabilization is used, in order to provide the fins ample space. There is however another reason why fin actuation is less practical for side-to-side configuration.

It has been shown in the previous chapter that actuation in heave using fins is not pratical. For bow-to-stern configuration the solution was actuation in pitch, and for side-to-side configuration the solution would be actuation in roll. This is less efficient. Since the ship is 16 meters wide, in order to lift one side of the ship 2 meters, it has to roll on an angle of $atan(2/8) = 14°$, which is about twice as much as pitch angle for the similar rise at bow or at stern. This can significantly reduce other seakeeping characteristics.

However, the force necessary to roll a typical ship is usually much less than the force necessary to pitch it. This means that smaller fins could be used in side-to-side configuration and yield some improvement in stabililty of the ramp.

3.3 Simulation

3.3.1 Physical model

In order to design a controller, a state space model is needed. The status of the project when this author joined was that the project was simulated in a Matlab package called SimMechanics. This package is an extension of simulink which allows simulation of mechanical blocks such as springs, rigid bodies, connections etc. The numerical values used were set so as to make simulation appear natural, without any other source.

In this section, a state-space model is developed. The physical model is based on Hamiltonian mechanics, due to similarity of the Hamiltonian function to Lyapunov function, and potential usage in proving stability. Although it is not assumed that the reader is familiar with the Hamiltonian Mechanics, this author can not hope to do any better than to refer the reader to either [13] or

[4]On a sidenote, one of the main cause of the present economic crisis is that people used financial models without properly understanding they were based on, thus accepting unrealistic results.

[12], both excellent publications covering the subject from somewhat different angles. If time constraints do not allow the reader to become familiar with those publications, he will have to take many of the stated equations for granted.

The purpose of this model is to provide a mathematical description of the dynamics to the controller. The model also has to create naturally-looking simulations.

Wave forces are then modeled as a combination of Response Amplitude Operators (RAOs). The motivation for this will be discussed below.

In general, a tremendous emphasis was given on *simplicity* of the model, as opposed to its *fidelity*. The reason for that is two-fold. First, although significant effort is put into research of nonlinear models for marine applications in the litterature, in practice simple linear models work just fine for most applications and non-linear models are highly unusual in the industry. The task of this project is to create a working solution using as simple means as possible, so implementation of complex nonlinear models is not necessary. Second, the only way to model a system that involves fluid dynamics with a reasonable precision is CFD, which can not be used for control (perhaps except for MPC, but running MPC on a CFD model is far ahead of the state of the art). This means that large increases in the complexity of the model may lead to little increase in its fidelity.

3.3.2 General setup of the model

For both Hamiltonian and Lagrangian mechanics, the complexity of the model is highly dependent on the state variables chosen to express a system. In this section, the state variables used to model this sytem are presented. This choice of state variables may appear odd, but it has in fact been thoroughly thought though in order to simplify simulation and controller design.

The full state vector is

$$x = \begin{bmatrix} x_1 & z_1 & \theta_1 & x_2 & z_2 & \theta_2 \end{bmatrix}^T \tag{3.14}$$

This vector consists of six variables, while the system only has five degrees of freedom. A choice is made to express x_2 in terms of other variables, and define vector q to consist exclusively of independent states:

$$q = \begin{bmatrix} x_1 & z_1 & \theta_1 & z_2 & \theta_2 \end{bmatrix}^T \tag{3.15}$$

Also, defining

$$\nu = \frac{d}{dt} q = \begin{bmatrix} \dot{x}_1 & \dot{z}_1 & \dot{\theta}_1 & \dot{z}_2 & \dot{\theta}_2 \end{bmatrix}^T \tag{3.16}$$

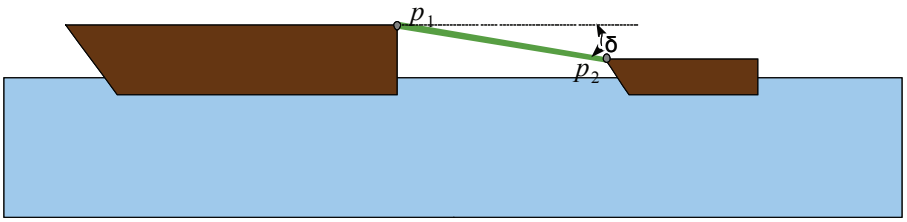

(a) Equilibrium position.

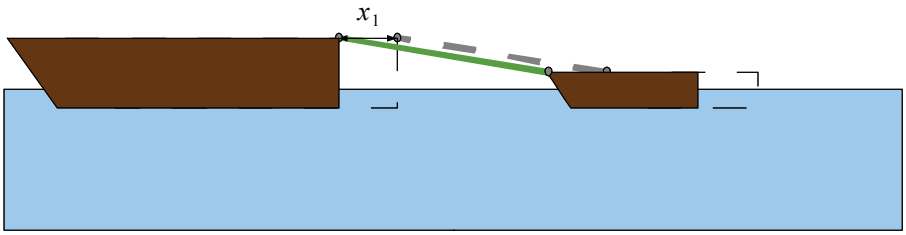

(b) The entire system has moved in surge.

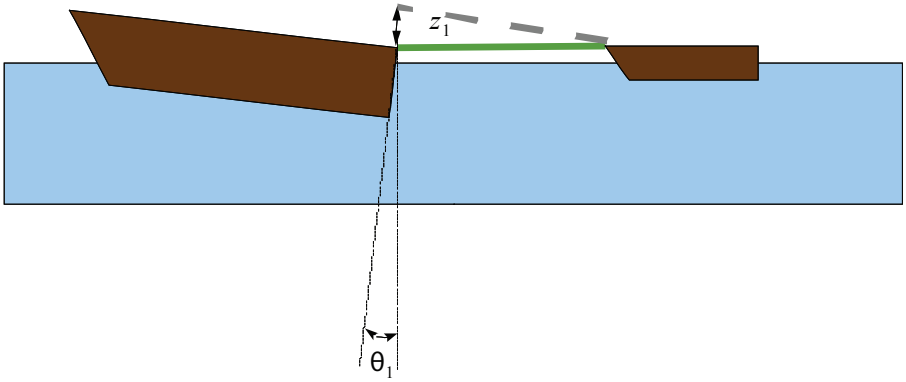

(c) The front ship has pitched, point p_1 is also dispalced in heave.

Figure 3.5: Illustration of state variables for the first ship. The variables are similar for the second ship.

The variables are independent and thus can be used as generalized coordinates. The variables in vector q figures 3.5 and 3.6 and table 3.3.

In the following, angles θ_1 and θ_2 will be assumed to be small enough for the linear approximations to be applicable.

3.3.3 Building up of the Hamiltonian function

In order to set up a Hamiltonian function, both potential energy and kinetic energy functions need to be stated as functions of the state variables.

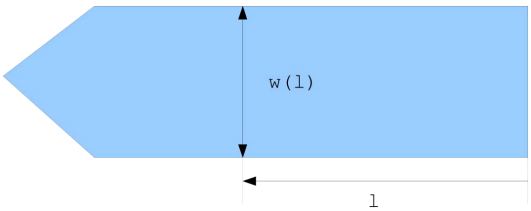

Figure 3.6: Horizontal cross-section of the ship, in the plane of where the water intersects the hull when the vessel is at equilibrium in calm water.

p_1	The point where the ramp is attached to the first vessel (Seabase)
p_2	The point where the ramp is attached to the first vessel (T-Craft)

Table 3.2: Definitions of the geometrical points on figure 3.5

3.3.3.1 Potential energy function

The effects of buoyancy and gravity are treated together as the restoring force. The calculations and assumptions are similar as those which led to (3.11). First potential energy for displacement in heave is calculated, then potential energy for pitch *around* p_1.

For heave, have, by integrating the force in (3.1) from zero to some heave displacement z, we get

$$V_{\rho,z} = \int_0^z LW\check{z}\rho_{sw} \cdot gd\check{z} = LW\rho_{sw}g\frac{z^2}{2} \tag{3.17}$$

For pitch displacement *around the Center of Buoyancy*, we integrate (3.11) from zero to an angle θ

$$\int_0^\theta \rho_{sw}g\,tan(\check{\theta})W\frac{L^3}{12}d\check{\theta} \approx \frac{1}{24}\rho_{sw}gWL^3\theta^2 \tag{3.18}$$

When the ship is rotated around p_1, center of buoyancy experiences a displacement in heave. The additional potential can be calculated using (3.17). The displacement in heave is approxiamtely $\theta\frac{L}{2}$, so the additional term will be

$$LW\rho_{sw}g\frac{L^2\theta^2}{8} = W\rho_{sw}g\frac{L^3\theta^2}{8} \tag{3.19}$$

Adding (3.18) and (3.19), yields

$$V_{\rho,\theta_1} = \frac{1}{24}\rho_{sw}gW_1L_1^3\theta_1^2 + W_1\rho_{sw}g\frac{L_1^3\theta^2}{8} = \frac{4}{24}\rho_{sw}gW_1L_1^3\theta_1^2 \tag{3.20}$$

Thus the total potential due to restoring forces for the Seabase is

$$V_{SB} = \frac{1}{2}L_1W_1\rho_{sw}gz_1^2 + \frac{1}{6}\rho_{sw}gW_1L_1^3\theta_1^2 \tag{3.21}$$

x_1	Position of the first vessel as measured at the point $p_1$where it is connected to the ramp. Positive direction forward
z_1	Vertical displacement of the point p_1 from its equilibrium position. Positive direction down.
θ_1	Rotation of the first vessel around point p_1. Positive direction is when the ship "sinks", as required for the right-hand coordinate system
x_2	Position of the second vessel as measured at the point $p_2$where it is connected to the ramp. Positive direction forward. In this representation, x_2 is not independent.
z_2	Vertical displacement of the point where the ramp is attached to the second vessel (similar to p_1 for the first vessel) from its equilibrium position. Positive direction down.
θ_2	Rotation of the second vessel around point where the ramp is attached to the second vessel (similar to p_1 for the first vessel). Positive direction is when the ship "rises", as required for the right-hand coordinate system

Table 3.3: Definitions of the state variables for the aft-to-fore ramp connection

The similar expression for the T-craft is

$$V_T = \frac{1}{2} L_2 W_2 \rho_{sw} g z_2^2 + \frac{1}{6} \rho_{sw} g W_2 L_2^3 \theta_2^2 \tag{3.22}$$

with the total potential energy being

$$V = V_{SB} + V_T \tag{3.23}$$

3.3.3.2 Kinetic energy function

To compute the kinetic energy of the vessels, mass tensors in the connection points between the bridge and the hulls are calculated. The lead vessel is given full freedom in 2D (3DOFs), while the second vessel is constrained in x.

The mass tensor in the point where the ramp is connected to the ship could be using either the formula (3.217) in TIF, or using the parallel axis theorem, which gives

$$T = \frac{1}{2} \check{\nu}^T \check{M} \check{\nu} \tag{3.24}$$

Where

$$\check{\nu} = \begin{bmatrix} \dot{x}_1 & \dot{z}_1 & \dot{\theta}_1 & \dot{x}_2 & \dot{z}_2 & \dot{\theta}_2 \end{bmatrix}^T$$

i.e. includes the dependent state x_2. In this setup,$\check{M}$ is the block-diagonal combination of the mass tensors of the two vessels expressed at the connection

point between the ramp and each of the vessels, which will be calculated in section 3.3.3.3.

Further, notice that for reasonably small Δz, defined as $\Delta z = z_2 - z_1$

$$x_2 \approx x_1 - l_r \cos(\delta) + \Delta z \tan(\delta) \tag{3.25}$$

The basis for this approximation is illustrated on Figure 3.7. Assumption that the ramp length varies slowly compared to the other variables gives

$$\dot{x}_2 \approx \dot{x}_1 + \Delta \dot{z} \tan(\delta) \tag{3.26}$$

In vectorial form,

$$\check{\nu} = \underbrace{\begin{bmatrix} 1 & 0 & 0 & 0 & 0 \\ 0 & 1 & 0 & 0 & 0 \\ 0 & 0 & 1 & 0 & 0 \\ 1 & -t(\delta) & 0 & t(\delta) & 0 \\ 0 & 0 & 0 & 1 & 0 \\ 0 & 0 & 0 & 0 & 1 \end{bmatrix}}_{Y} \nu = Y\nu$$

where $t(\delta) = tan(\delta)$ and ν defined in (3.16). This allows transforming (3.24) to

$$T = \frac{1}{2}\nu^T \underbrace{Y^T \frac{1}{2}\left((\check{M} + \check{M}^T) + (\check{M} - \check{M}^T)\right) Y}_{M} \nu = \frac{1}{2}\nu^T \underbrace{Y^T \frac{1}{2}\left(\check{M} + \check{M}^T\right) Y}_{M} \nu = \frac{1}{2}\nu^T M \nu \tag{3.27}$$

Notice that M is positive definite as long as $\check{M}$ satisfies $x^T \check{M} x > 0 \forall x \neq 0$. This is necessary because, although physical mass tensor is always positive definite, *added mass*, which is used to represent the part of the hydrodynamic force proportional to acceleration, in general is not symmetric. This will be discussed further in subsection 3.3.3.3.

The standard procedure to derive $\dot{q}$ is using (3.38). However, since in this case T is expressed as function of \dot q$H(q, p, t) = V(q) + T(p)$, and the conjugate momenta p is defined in [12] (2.44) as

$$p = \frac{\partial L}{\partial \dot{q}} = \frac{\partial T(\dot{q}) - V(q)}{\partial \dot{q}} = \frac{\partial T}{\partial \dot{q}}$$

we have that

$$p = M\dot{q} \tag{3.28}$$

$$\nu = \dot{q} = M^{-1} p \tag{3.29}$$

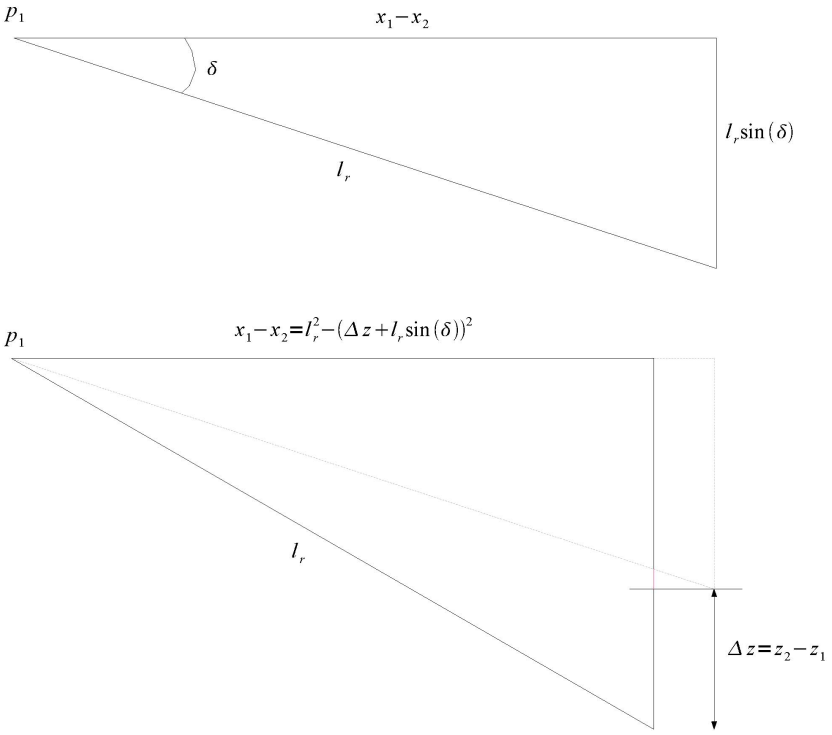

Figure 3.7: Drawing on top is an illustration of the connection in the equilibrium position with $z_1 = z_2 = 0$. When z_2 deviates from the equilibrium, the dependent variable $x_2$must also change. l_r is the length of the ramp. This approximation discards the part of triangle shown in red.

Some readers will insist on using Hamiltonian equations thoughout the derivation. To accomodate those, setting up

$$\begin{aligned}\dot{q} &= \frac{\partial H(q,p,t)}{\partial p} = \frac{\partial (T(p)+V(q))}{\partial p} \\ &= \frac{\partial T(p)}{\partial p} = \frac{\partial (\frac{1}{2}p^T M^{-T} M M^{-1} p)}{\partial p} = M^{-T}p = M^{-1}p.\end{aligned}$$

Which is same as (3.29).

3.3.3.3 Calculating the mass

The mass tensor $\check{M}$ in (3.24) is a block-diagonal combination of the two-dimensional mass tensors of the two vessels expressed at the points where the ramp is attached to the vessels. To calculate those, let M_1^p and M_2^p be the generalized mass tensors in the xz-plane of the sea base and of the T-craft respectively given on arbitrary points on those crafts, p_1 and p_2 (not to be confused with similarly named points on Figure 3.5). Next, let $\vec{r}_{p_1}$ and $\vec{r}_{p_2}$ be vectors from attachment points of the ramp to the points p_1 and p_2 . By application of [6] equation (3.217) and substitution into the formulas above,

$$\check{M} = \begin{bmatrix} H^T(\vec{r}_{p_1}) M_1^{\mathrm{p}} H(\vec{r}_{p_1}) & 0 \\ 0 & H^T(\vec{r}_{p_2}) M_2^{\mathrm{p}} H(\vec{r}_{p_2}) \end{bmatrix}$$

Where $H(r)$ is given by [6] equation (3.210).

3.3.4 Listing of the partial derivatives

In this section, the partial derivatives are listed for the purpose of being implemeted in a computer model.

$$q = \begin{bmatrix} x_1 & z_1 & \theta_1 & z_2 & \theta_2 \end{bmatrix}^T \tag{3.30}$$

$$\nu = \dot{q}$$

$$p = M\nu$$

For this particular application, Hamiltonian was checked to be $H = T+V$. Since $T(p)$ does not depend on q explicitely, and $V(q)$ does not depend on either p or ν, we have $\frac{\partial H}{\partial q} = \frac{\partial V}{\partial q}$ and $\frac{\partial H}{\partial p} = \frac{\partial T}{\partial p}$. Writing out the Hamiltonian equations of motion:

$$-\dot{p}_1 = \frac{\partial V}{\partial x_1} = 0 \tag{3.31}$$

$$-\dot{p}_2 = \frac{\partial V}{\partial z_1} = L_1 W_1 \rho_{sw} g z_1 \tag{3.32}$$

$$-\dot{p}_3 = \frac{\partial V}{\partial \theta_1} = \frac{1}{3}\rho_{sw} g W_1 L_1^3 \theta_1 \tag{3.33}$$

$$-\dot{p}_4 = \frac{\partial V}{\partial z_2} = L_2 W_2 \rho_{sw} g z_2 \tag{3.34}$$

$$-\dot{p}_5 = \frac{\partial V}{\partial \theta_2} = \frac{1}{3}\rho_{sw} g L_2^3 W_2 \theta_2 \tag{3.35}$$

And finally

$$\dot{q} = \nu = M^{-1} p \tag{3.36}$$

Notice that the formulation above exclues any hydrodynamic forces or actuation.

3.3.5 Numerical values

In order to do a meaningful computer simulation of the system, there is a need for realistic numerical values for a lot of parameters, such as ship's mass, the hydrodynamic damping coefficients including the added mass, moments of inertia et cetera. An attempt was made to find data for similar ships on the Internet, however, no satisfactory data was found available.

However, the GNC Matlab toolbox provided by Marine Systems Simulator developement group provides models for a wide range of ship types, non-dimensionalazied by Prime-system I (see [6] page 313). The model for mariner class vehicle was used for both Seabase and T-craft, dimensionalized with the ships' length in Table 3.1.

3.3.6 Other forces

The forces listed in Section 3.3.4 is not complete in the sence that it does not include the hydrodynamic and actuation forces.

Lagrange's equations, the way they are set up in [12], allow to add a generalized force which either are not derivable from a scalar potential or not included in the scalar potential for other reasons using

$$\frac{d}{dt}\left(\frac{\partial L}{\partial \dot{q}_j}\right) - \frac{\partial L}{\partial q_j} = Q_j \tag{3.37}$$

where $L = T - V$ and Q_j are the generalized forces that are not included in potential V. The equation is valid for every degree of freedom j. Goldstein did not provide any similar device the Hamiltonian Mechanics. Those will be derived in the following theorem

Theorem 3.1. *With Hamiltonian defined as $H = p_i\dot{q}_i - L$ and in presence of generalized force Q_j, the Hamiltonian equations of motion can be set up as follows*

$$\begin{aligned} \dot{p}_j &= -\frac{\partial H}{\partial q_j} + Q_j \\ \dot{q}_j &= \nu_j = \frac{\partial H}{\partial p_j} \end{aligned} \tag{3.38}$$

Proof. Although this equation was shown by the author independently, this theorem was undoubtedly known for centuries. For this reason, only a rough outline of the proof will be given. It is similar to proof presented in [12] for the same statement without the generalized force. In [12], equation (3.37) is used without the generalized force on the right hand side to deduce the differential dH, i. e

$$\frac{\partial L}{\partial q_j} = \frac{d}{dt}\left(\frac{\partial L}{\partial \dot{q}_j}\right) = \dot{p}_j \tag{3.39}$$

Accounting for Q_j in (3.37), (3.39) is transformed to

$$\frac{\partial L}{\partial q_j} = \dot{p}_j - Q_j \tag{3.40}$$

changing the differential dH to

$$dH = \dot{q}_j\, dp_j - (\dot{p}_j\text{-}Q_j)\, dq_j - \frac{\partial L}{\partial t}\, dt \tag{3.41}$$

yielding

$$\frac{\partial H}{\partial q_j} = \text{-}(\dot{p}_j\text{-}Q_j) \tag{3.42}$$

thus proving (3.38).

□

3.3.6.1 Actuator Forces

The actuators on this system are the main propellers on both ships, and the fins on the second vessel, configured so as to act only in pitch. The input vector is defined as

$$\tau = \begin{bmatrix} \tau_{x_1} & \tau_{x_2} & \tau_{pitch} \end{bmatrix} \tag{3.43}$$

with τ_{x_1} being the force from the propeller on the seabase, τ_{x_2} the force from probeller on the T-craft, and τ_{pitch} is the torque on the T-craft created by the fins.

The propeller on the second vessels acts along the direction of the generalized co-ordinate x_1 , but the other two actuators do not act along any generalized co-ordinate. A generalized force Q_j in direction of the generalized coordinate j is defined per

$$Q_j = \sum_i F_i \frac{\partial x_i}{\partial q_j} \tag{3.44}$$

According to (3.25), the value of x_2 is a function of x_1 , z_1 and z_2. A mathematically rigorous analysis would include the second propeller's contribution in directions z_1 and z_2 . However, it is apparent from the practical considerations that a force the second propeller could practically generate is not going to force the T-craft significantly down and especially not force the sea base up. Because of the ramp, τ_{x_1} and τ_{x_2} are acting essentially in the same degree of freedom, and should be coordinated so as to limit the strain on the ramp.

In vectorial form, the generalized force from the actuators is

$$Q_\tau = \begin{bmatrix} 1 & 1 & 0 \\ 0 & 0 & 0 \\ 0 & 0 & 0 \\ 0 & 0 & 0 \\ 0 & 0 & 1 \end{bmatrix} \tau \tag{3.45}$$

Notice that the matrix does not have full rank.

3.3.6.2 Hydrodynamic damping forces

In the general form usually used in maritime literature, the hydrodynamic force F_H for a solid body moving through a fluid is a function of velocity and acceleration in six degrees of freedom, i.e.

$F_H = F_H(\nu, \dot{\nu}) \in \mathbb{R}^6$

where ν is the velocity in the Body coordinate system following the SNAME standard. In this application, the ships' position in the water is also relevant, because a ship that is "lifted" out of the water in general has its drag reduced. The F_H itself is non-linear and highly coupled. In hydrodynamic control applications, the hydrodynamic force is usually linearized, sometimes with the second degree polynomial used on surge direction where the speed may be significant. We can set this up as following

$$F_H(\nu, \dot{\nu}) = \underbrace{\frac{\partial F_H}{\partial \dot{\nu}}}_{-M_A} \dot{\nu} + \underbrace{\frac{\partial F_H}{\partial \nu}}_{-D} \nu = -M_A \dot{\nu} - D\nu + h.o.t. \tag{3.46}$$

In the equation above linearization has to be performed at ($\nu = 0$, $\dot{\nu} = 0$), but this doesn't have to be the case in general. M_A is so-called *Added Mass*, which arises because movement of a body creates motion in fluid that would not be present there otherwise. An interesting point is that no concept of added mass exists in aerodynamics. This is due to different densities of working fluids in that discipline - even though air is moving in same pattern due to flows being similar, the momentum carried by the air is much less than that of water.

In an ideal fluid M_A is constant with speed, but varies with encounter frequency with waves. It thus resembles the mass tensor that was discussed above. Unless certain symmetries are present, the added mass tensor does not possess a structure of any particular interest, except that $M_A + M_A^T$ is positive definite. In control application we often consider the "total mass" of a marine vessel as sum of its physical mass and the added mass.

Damping force is both non-linear and coupled, and given the other concerns mentioned above it can only be guessed upon. That is exactly what is done in this work. Damping tensor is modeled as diagonal at CG of each ship, then moved to the points of ramp connection using equations in [6], section 3.4:

$$\check{F}_{H,D} = -D_{\text{CG}}\nu_{\text{CG,1-ship}} = -H^T(r_{CG,1})D_{CG}H(r_{CG,1})\check{\nu}_{1-ship}$$

for one ship; for two ships two-ship system the force is

$$\check{F}_{H,D} = -\underbrace{\begin{bmatrix} H^T(r_{CG,1})D_{CG,1}H(r_{CG,1}) & 0 \\ 0 & H^T(r_{CG,2})D_{CG,2}H(r_{CG,2}) \end{bmatrix}}_{\check{D}} \begin{bmatrix} \check{\nu}_1 \\ \check{\nu}_2 \end{bmatrix} = -\check{D}\check{\nu}$$

Transforming to generalized force:

$$Q_{H,D} = \frac{\partial x}{\partial q}^T \check{F}_{H,D} = Y^T\check{F}_{H,D} = -Y^T\check{D}\check{\nu} = -\underbrace{Y^T\check{D}Y}_{D}\nu = -D\nu \tag{3.47}$$

The total generalized force coming from hydrodynamic damping and from actuators is thus

$$Q = Q_\tau + Q_{H,D} \tag{3.48}$$

3.3.7 Wave forces

The waves that are of interest in engineering applications is a gravitational phenomenon. If fluid acquires potential energy, then the continuity, energy conservation and pressure equilibrium conditions imply that the energy will be spread in the fluid as waves. Deriving models for undisturbed waves is a non-trivial, but tractable task if certain linearizations and a few other approximations are allowed. Interaction between the waves and the hull of a vessel is even more

complicated and can only be done using CFD simulations. This approach is not directly applicable to control task.

Instead, the approach based on model in [6] (6.62)-(4.64) is used, with wave forces modeled as second-order colored noise acting as on the vessel as Response Amplitude Operator (RAOs). This approach was preferred to use of force transfer functions out of practical considerations for this particular problem - when a wave lifts a ship, the action more resembles a spatial displacement than a force. In other problems, wave action in different DOFs, such as yaw and sway, is modeled, and FAO may be considered more appropriate.

As such, waves are modeled as either (4.50)- (4.53) or (4.54)-(4.55) in [6], in both cases

$$\dot{x}_w = A_w x_w + e_w w_w \tag{3.49}$$

$$y_w = c_w^T x_w \tag{3.50}$$

with an independent system for each of the five degrees of freedom. The values of A_w, e_w and c_w are given in [6] and will not be reiterated here.

3.3.8 Controller

The available model of the system is very coarse, so any controller to be used needs to be robust with respect to models that are not robust. Also, the fact that this is a five-dimensional system, makes LQR an apparent choice for a controller.

In order for an LQR controller to work, the system needs to be either controllable or stabilizable. In the following, it will be proven that the system is in fact stable.

Theorem 3.2. *The unforced system (3.31)-(3.36) excluding the surge degree of freedom and including the damping is asymptotically stable.*

Proof. Since Hamiltonian is in this case sum of energies, it must be at least positive semi-definite. Obviously, kinetic energy can only be zero if there is no movement. Mathematically, since $H = T + V$, we have that $T = \frac{1}{2}\nu^T M \nu$ is positive definite because M is positive definite. V is also obviously positive definite by inspection of (3.21)-(3.23).

The time derivative of the Hamiltonian will be shown to be negative semidefinite:

$$\frac{dH(q,p,t)}{dt} = \frac{\partial H}{\partial q}^T \frac{dq}{dt} + \frac{\partial H}{\partial p}^T \frac{dp}{dt} + \frac{\partial H}{\partial t} \tag{3.51}$$

Substituting $\frac{\partial H}{\partial p}$ using the first part of (3.38) and $\frac{dp}{dt}$ with the second part of (3.38), and using that the Hamiltonian is not explicitely dependent on time, have

$$\frac{\partial H}{\partial q}\frac{dq}{dt} + \frac{\partial H}{\partial p}\frac{dp}{dt} + \underbrace{\frac{\partial H}{\partial t}}_{0} = \frac{\partial H}{\partial q}\dot{q} + \dot{q}\left(-\frac{\partial H}{\partial q} + Q\right) \tag{3.52}$$

Now, using that $Q = Q_{H,D} = -D\nu = -D\dot{q}$ for an unforced system. Also, since damping is positive definite, we have that

$$\frac{dH}{dt} = -\dot{q}^T D\dot{q} \tag{3.53}$$

This proves that $\dot{H}$ is negative *semi*definite, not negative definite, since it is also a function of p.

However, examination of equations (3.31)-(3.35) shows that the system can not remain in $p = M\dot{q} = 0$ unless $q = 0$, proving stability per Krasovskii theorem.

□

3.3.8.1 Model setup

In order to design a simulation, it is desired to present the model as a linear system in the matrix form $\dot{x} = \mathbf{A}x + \mathbf{B}u$. This is done in the present section.

First, let vector $\mathbf{p}$ be the combination of generalized momenta $p_1 \dots p_5$, and q still defined as $q = \begin{bmatrix} x_1 & z_1 & \theta_1 & z_2 & \theta_2 \end{bmatrix}^T$. (3.31)-(3.35) and (3.45), can now be combined to

$$\begin{aligned}\dot{\mathbf{p}} &= \underbrace{-\rho_{sw} g \begin{bmatrix} 0 & 0 & 0 & 0 & 0 \\ 0 & L_1 W_1 & 0 & 0 & 0 \\ 0 & 0 & \frac{1}{3} W_1 L_1^3 & 0 & 0 \\ 0 & 0 & 0 & L_2 W_2 & 0 \\ 0 & 0 & 0 & 0 & \frac{1}{3} W_2 L_2^3 \end{bmatrix}}_{\Gamma} \mathbf{q} - D\nu + \underbrace{\begin{bmatrix} 1 & 1 & 0 \\ 0 & 0 & 0 \\ 0 & 0 & 0 \\ 0 & 0 & 0 \\ 0 & 0 & 1 \end{bmatrix}}_{B} \tau \\ &= \Gamma \mathbf{q} - D\nu + B\tau \end{aligned} \tag{3.54}$$

Also, per (3.36).

$$\dot{q} = \nu = \mathbf{M}^{-1} p \tag{3.55}$$

Combining (3.54) and (3.55),

$$\begin{bmatrix} \dot{p} \\ \dot{q} \end{bmatrix} = \begin{bmatrix} -DM^{-1} & \Gamma \\ M^{-1} & 0_{5x5} \end{bmatrix} \begin{bmatrix} p \\ q \end{bmatrix} + \begin{bmatrix} B \\ 0_{5x3} \end{bmatrix} \tau \tag{3.56}$$

3.3.8.2 Controller

The controller to be designed needs to be optimal with respect to difference between heights of the attachment points, namely $z_2 - z_1$. This is equivalent to minimizing the roll angle of the ramp, since $z_2 - z_1$ is a diffeomorphism of the roll angle. To accomplish that, we need a representation of (3.56) which includes $z_2 - z_1$. This is done with a linear state transformation

$$\breve{q} = \underbrace{\begin{bmatrix} 1 & 0 & 0 & 0 & 0 \\ 0 & 1 & 0 & 0 & 0 \\ 0 & 0 & 1 & 0 & 0 \\ 0 & -1 & 0 & 1 & 0 \\ 0 & 0 & 0 & 0 & 1 \end{bmatrix}}_{\Lambda^-} = \Lambda^- q \tag{3.57}$$

and

$$\begin{bmatrix} p \\ \breve{q} \end{bmatrix} = \underbrace{\begin{bmatrix} I_{5x5} & 0 \\ 0 & \Lambda^- \end{bmatrix}}_{\Lambda} \begin{bmatrix} p \\ q \end{bmatrix} = \Lambda \begin{bmatrix} p \\ q \end{bmatrix}$$

This allows transforming (3.56) to

$$\begin{bmatrix} \dot{p} \\ \dot{\breve{q}} \end{bmatrix} = \Lambda \begin{bmatrix} -DM^{-1} & \Gamma \\ M^{-1} & 0 \end{bmatrix} \Lambda^{-1} \begin{bmatrix} p \\ \breve{q} \end{bmatrix} + \Lambda \begin{bmatrix} B \\ 0_{5x3} \end{bmatrix} \tau$$

Since those equations are linear, both simulation and design of an LQR controller is a trivial task and will not be discussed in a great detail; an interested reader can refer to the code on the attached DVD. The result of the LQR algorithm is a matrix K, so that controller becomes

$$\tau = K \begin{bmatrix} p \\ \breve{q} \end{bmatrix} = K\Lambda \begin{bmatrix} p \\ q \end{bmatrix}$$

3.4 Results

Figure 3.8 shows behavior of the system in the unactuated and actuated case. The dashed red line showing the difference in displacement of the attachment points. In unactuated case, this difference goes up to 2.2 meters, while in actuated case this difference is reduced to 0.7 meters. This is a clear improvement.

Figure 3.9 shows the torque that the fins are required provide in order to change the behavior of the system from Figure 3.8a to 3.8b. This is interesting, because while the preliminary results from Section 3.2 are calculations based on how much force is required to keep a ship in certain constant displacement in water, Section 3.3 produces results from simulation with relatively realistic models for waves and for the ships in a more realistic situation. The maximal torque the fins need to output is $60MN \cdot m$. Each fin is about 20 meters from the Center

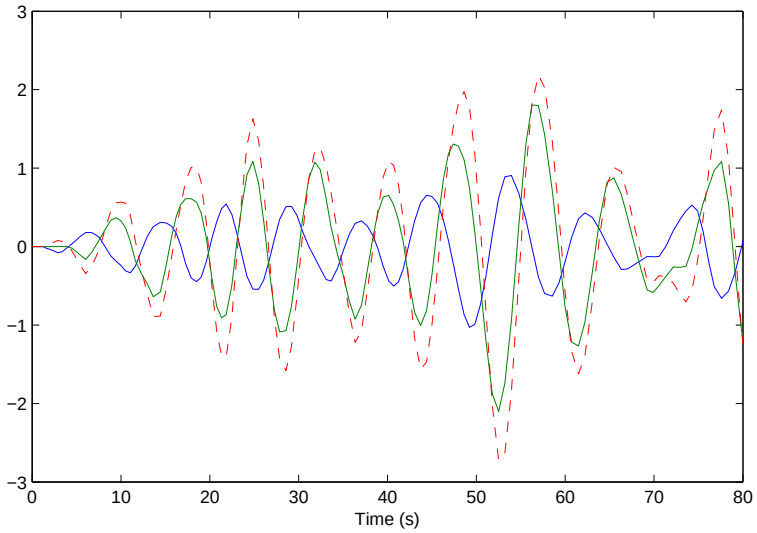

(a) Unactuated case. The maximal difference between the connection points is 2.2 meters

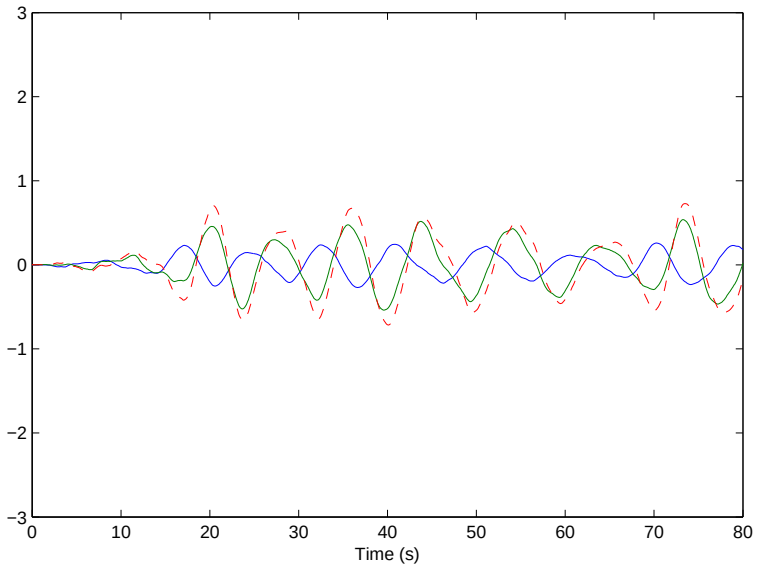

(b) Unactuated case. The maximal difference between the connection points is now 0.7 meters

Figure 3.8: The system before and after actuation. The green line shows the vertical movement of the connection point between the T-craft and the ramp, the blue line similarly shows the connection between the ship and the seabase, and the red dashed line shows the difference.

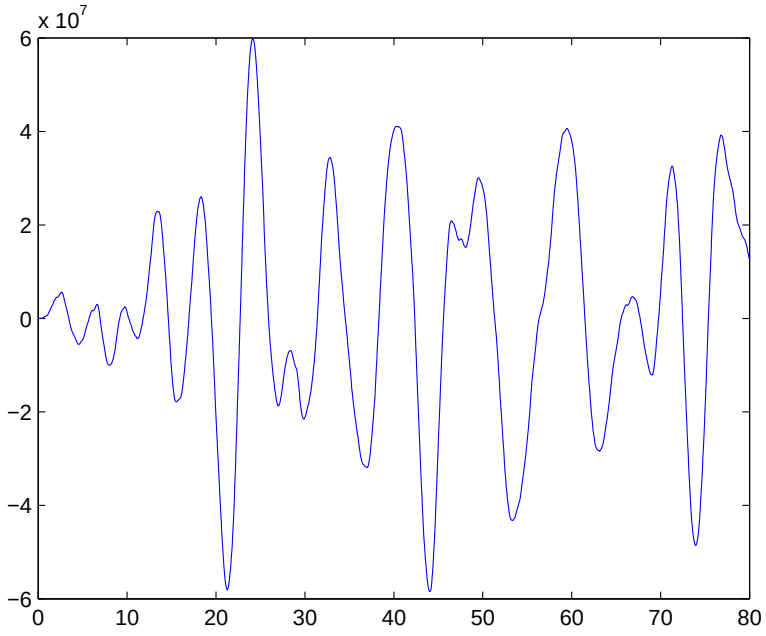

Figure 3.9: Required torque, $MN \cdot m$

of Gravity on the T-craft (ref Table 3.1). Thus, the total force to be produced by the fins is $3MN$, which is somewhat lower than the figure of $4.3MN$ from the preliminary analysis. Consequently, the fins that are required are somewhat smaller. Again using (3.4), the total fin area needed is $48m^2$, and four fins $1.4m \times 8.5m$ are engough to do the job.

This is of course somewhat arbitrary, since there is a tradeoff between the degree of dampening and the size of the fins. Still, the nature of this tradeoff has been clearly illustrated.

3.5 Conclusion and suggestions for future research

In this section, the possibility of actuating the T-craft with fins was examined and estimates for needed fin size have been made. Although the estimation work had to be rough due the system being in conceptual stage, the results achieved suggest that a fin-actuated T-craft can in fact be built, and it would yield significant boost in overall system performance.

This idea has not been proposed before and was received with significant interest. It has been presented for the Office of Naval Research conference on February 4th, 2009 by Miroslav Krstić, and it will also be presented at 2009 Conference on Grand Challenges in Modeling and Simulation (GCMS'09) in Istambul.

There are quite a few opportunities to pursue the active control of the T-craft

further. Current design limits the attachment points so that the ships cannot roll independently. If this requirement is lifted, so that the pitch of the ramp follows the roll of the T-craft, the fins could be used to stabilize the ramp in pitch, as well as in roll. Another possible direction is to use a Surface Effect Vehicle for the T-craft, and actuating its heave by changing the air pressure in its cushion. Also, the attachment points between the ramp and the ships could be mounted on a heave-compensated platform. All in all, there are exciting and promising opportunities for further research.

Chapter 4

Side-To-Side Configuration

Unlike the previous chapter, this chapter deals with a configuration where ships sail side-to-side, with the ramp extending from starboard of one vessel to the port of the other. Since one of the vessels is much larger than the other, it opens up for a possibility of the larger ship shielding the smaller one from the waves. This involves a trade-off: most ship designs are least affected by the waves when heading straight into the wave fronts. When waves are coming from side, even large ships tend to become very sensitive to the waves. This means that there is an optimal angle ψ^* at which the ramp has least undesired movement, according to some performance criterion $f(\cdot)$ which is assumed has a minimum f^* at ψ^*.

An extremum-seeking based controller will be designed in this chapter to find angle ψ^* dynamically. The first section proposes a simple model for the system. It desired that the extremum-seeking controller concentrates on finding the optimal yaw angle ψ^*. Thus, a simple linear controller is designed to bring the ship system at a specified angle.

Then, reader is introduced to various techniques of extremum seeking. While the reader is still highly recommended to read the excellent introduction in [1], introduction in this work covers the subject from a different angle, with intention of reducing the effort for the reader, and potentially also making the technique accessible for a wider audience.

Section 4.5 desrcibes a technique for extending extremum seeking to systems with a certain class of uncertainties. This technique is original contribution of this thesis.

This technique is then applied to the ship model described in Section 4.1, and results are discussed.

4.1 Physical model and stabilizing controller

The system to be designed consists of a large ship and a small ship. Usually, this means that the smaller ship is more maneuverable than the large one, and a controller can be set up to make the small ship follow the large one. Results from

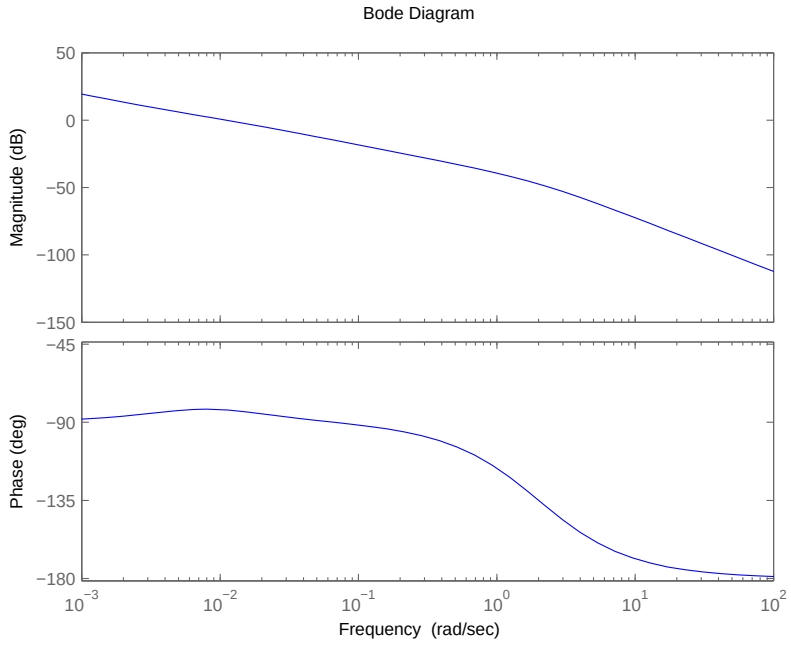

Figure 4.1: Open loop Bode diagram of controller (4.1) and system (4.2). Phase lag never goes below 180°.

[9] or [10] can be applied here. Only the dynamics of the larger ship are modeled here. Neither does this work intend to develope any kind of high-performance navigation controller. Thus, for this purpose, the linear second order Nomoto model is considerered suffisient. It connects the ship's rudder angle δ and yaw angle ψ per

$$\frac{\psi}{\delta}(s) = \frac{K}{s(1+Ts)} \tag{4.1}$$

where , for a mariner class vessel, $T = 107.3$s, and $K = 0.185$. This model is the most popular model for ship autopilot design due to its simplicity and accuracy ([6] p 309).

An extremum seeking controller is capable of handling time-variant maps. It is therefore possible to put 4.1 directly into the extremum seeking loop, and this type of system has indeed been tested and worked as a part of research for this thesis. However, to make the solution more clean, the task of taking the system to ψ^* is accomplished with a separate linear controller, while the extremum-seeking controller is left with the task of finding ψ^*. An integrator is already present in the system, so a PD controller is selected, with $T_d = 14$s, $K_p = 0.1$, and implemented as

$$G(s) = \frac{(T_d + K_p)s + K_p}{s+2} \tag{4.2}$$

The denominator $s + 2$ is there to make the controller proper and thus implementable. An open-loop Bode diagram of controller and system is shown on Figure 4.1.

A cost function needs to be modeled as a function having a minimum at some unknow value of ψ between zero and $\pi/2$. Function $f(\psi) = (\psi - 0.4)^2$ is chosen.

4.2 Introduction to Extremum Seeking

A reader who is not familiar with Control Theory or the higher mathematics in general could be inclined to believe that Extremum Seeking involves something like parachuting, expeditions to high mountains or handling poisonous snakes. This is however not the kind of extremes pursued in the present work. Instead, Extremum Seeking is a real-time optimization technique used for a class of problems where there exist a cost map $f(\theta) \in \mathbb{R}$ with $\theta(t) \in \mathbb{R}^N$ having a possibly time-varying extremum $f^*(t)$ at $\theta^*(t)$. The goal of an extremum seeking controller is to keep the output of this map close to that extremum.

This is not very hard to do for a memoryless SISO system. A simple scheme from [2] will be repeated in the next section. Extremum Seeking as presented in [1] can handle more complicated plant dynamics and also the seeking perturbations on it are more smooth. It superposes a harmonic modulation signal on the input signal of the plant, and uses the resulting periodic perturbations in the output signal to "navigate" towards the extremum point in the plant dynamics. If phase lag on the modulation frequency is not known exactly or is not constant, the Extremum Seeking controller may become unstable if error is sufficiently large. In particular, if the uncertainty reaches 180°, ES is guaranteed to move away from the extremum.

The major contribution of this chapter is a scheme that tracks the phase lag on the modulation frequency.

4.3 Extremum Seeking Scheme for a memoryless SISO system

An extremum could be either a minimum or a maximum. The theory, both in the present work and in [1], limits itself to looking for a minimum. This does not result in any loss of generality, since a maximum problem can be turned into a minimum problem by multiplying output with -1. Consider a memoryless SISO system with input $\theta(t) \in \mathbb{R}$ and output $f(\theta) \in \mathbb{R}$, with $f(\theta)$ having a clear, possibly time-dependent, minimum at $f^*(t)$. Algorithm 4.1 will keep the system close to this minimum. An example of execution is shown on Figure 4.2.

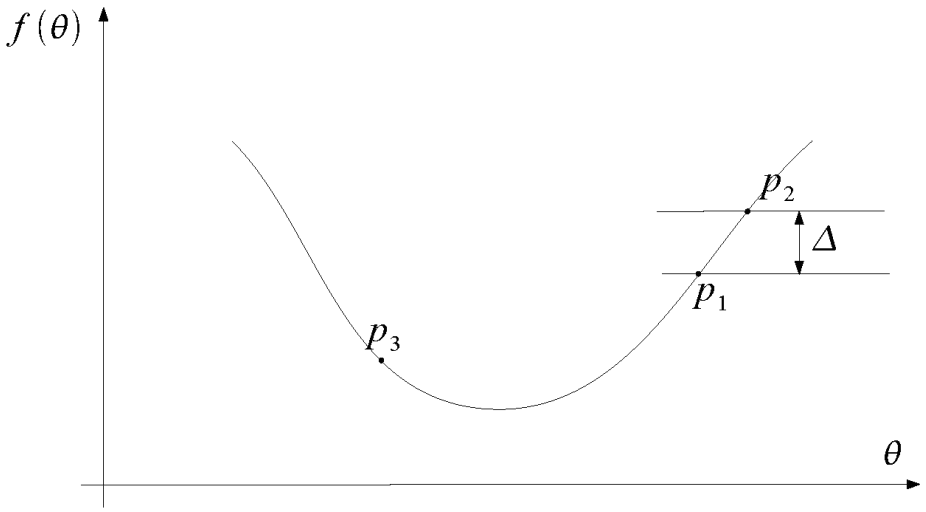

Figure 4.2: An example for execution of a simple extremum seeking scheme on a memoryless SISO map. Algorithm starts at point p_1 and initial v being positive. This means that the plant is initially moving away from the minimum of the map. Because $f(\theta)$ is increasing, f_m will stay at $f(\theta(p_1))$, and $f(\theta(t)) - f_m$ will increase until the threshold is reached at p_2. The direction of θ turns around and $f(\theta)$ goes towards the extremum while keeping $f_m = f(\theta)$. The plant will pass the extremum. When this happens f_m will stay at the minimal value, and $f(\theta(t)) - f_m$ will increase again until the threshold value is reached at p_2.

Algorithm 4.1 Extremum Seeking on memoryless SISO system

1. Start with some initial guess for θ, set v to some practically appropriate rate of change of θ, and $t_t = t_0$
2. Set $\dot{\theta} = v$ and apply the resulting signal θ on the plant, while remembering the minimal value of output $f(\theta)$, so that

$$f_m = \underset{t \geq t_t}{min} f(\theta) \tag{4.3}$$

3. If $f(\theta) - f_m > \Delta$, with Δ being some practical threshold value, then it is determined that the controller is moving the plant away from the minimum. Turn the plant around by setting $v \leftarrow -v$. Reset the minimal recorded value f_m by setting t_t to the current time t (time of turn), ie $t_t \leftarrow t$ and per (4.3) $f_m \leftarrow f(\theta(t))$. Go back to step 2, which now moves the plant in the opposite direction.

This technique can be extended to MISO system $f(\theta_1, \theta_2, \ldots, \theta_n)$ taking turns in changing directions of thetas. The details of this will however not be included in this work.

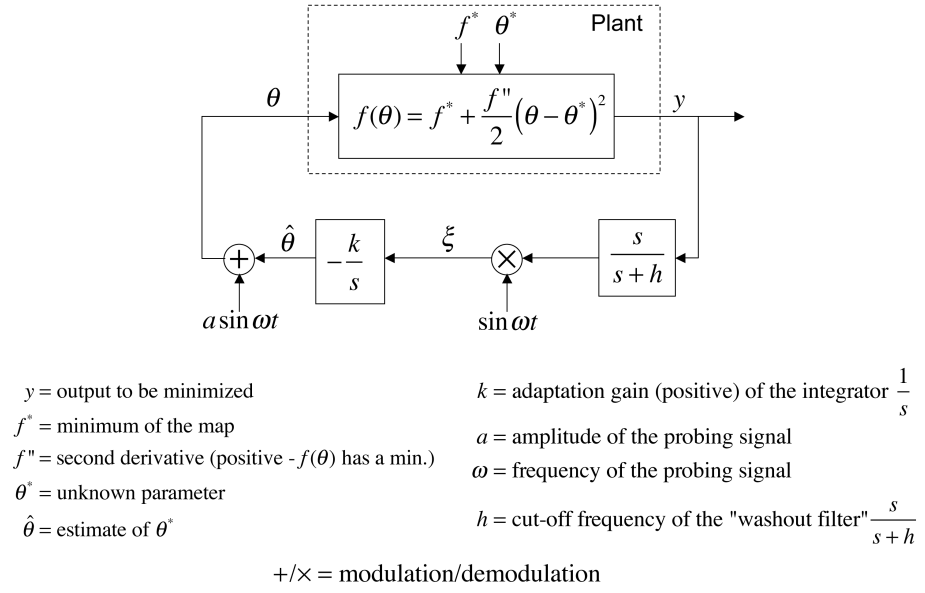

Figure 4.3: Simplified Extremum Seeking Scheme. Copyright: Miroslav Krstic

4.4 Extremum Seeking with harmonic modulation signal

An guide to Extremum Seeking is available in a "Real-Time Optimization by Extremum-Seeking Control", an excellent book co-authored by Kartik B. Ariyur and Miroslav Krstić. Chapter 1.1 provides a greatly simplified introduction.

This work aims to present an even more simplified introduction. It takes matters further by approximating the cost map as a piecewise-linear function shown on Figure 4.5, instead of second order (Taylor expansion) polynomial approximation which is used throughout [1]. The diagram of the method is shown on Figure 4.3. It also defines the variables to be used throughout this chapter.

Propagation of the signal through the system is shown on Figure 4.6 for values of θ where $f(\theta)$ has negative slope, i.e. the estimate $\hat{\theta}$ is too small. It is shown that in this case, ξ will remain negative thus increasing the value of $\hat{\theta}$. For values of θ where $f(\theta)$ has negative slope, the situation is opposite, ξ will remain positive and $\hat{\theta}$ declines. This is illustrated on 4.7.

The challenges for the engineer implementing the above scheme are:

- Finding a probing frequency ω high enough to allow quick convergence (low frequency = slow controller), but still low enough to allow the plant enough time to respond.
- Finding an amplitude of the probing signal large enough for the perturbations in the plant output to dominate measurement noise, while not disturbing the operation of the plant significantly.

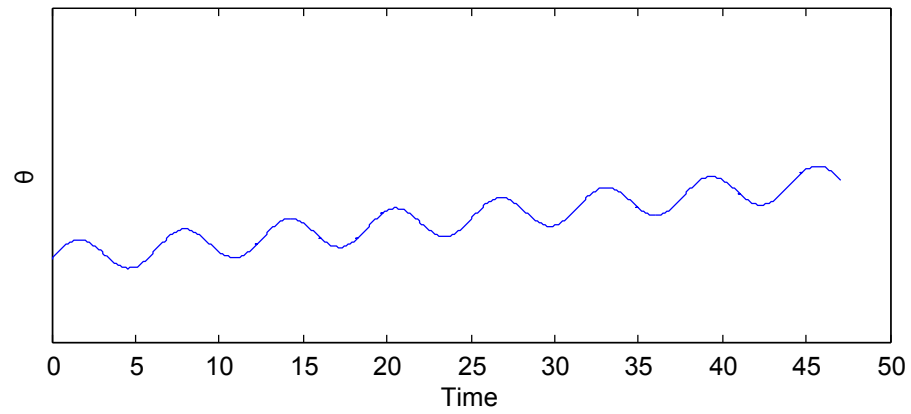

Figure 4.4: An example of signal θ. Signal$\hat{\theta}$ is assumed to vary slowly due to an integrator before it.

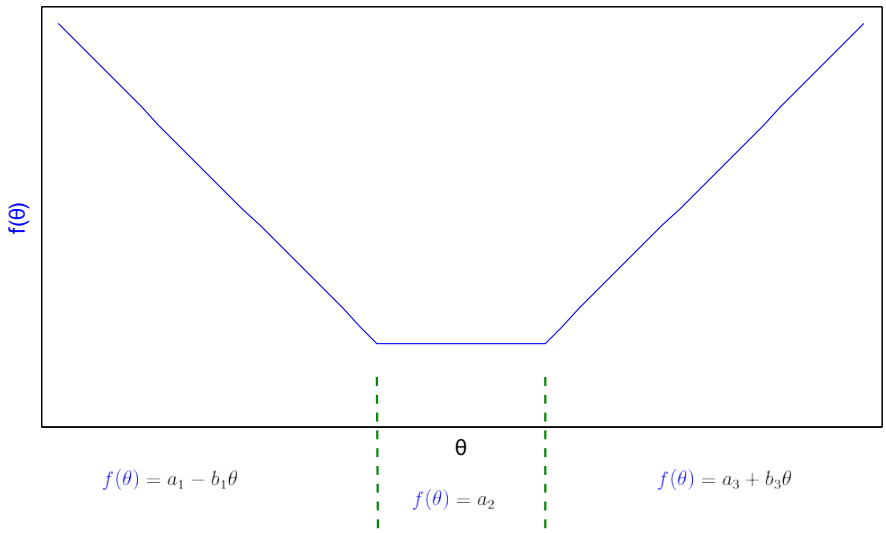

Figure 4.5: Approximation of $f(\theta)$in proximity of the extremum, in this case a minimum. While [1] uses a second order polynomial, this approximation is piecewise linear.

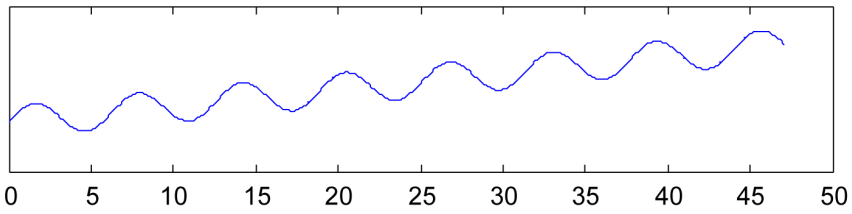

(a) The signal θ, same as on Figure 4.4.

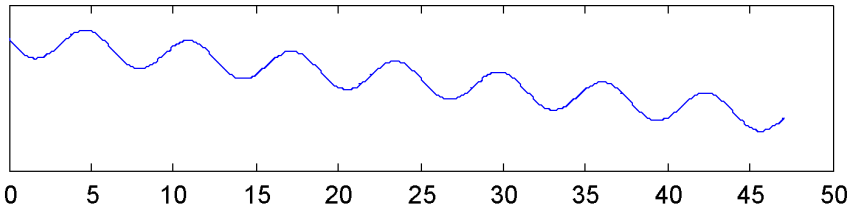

(b) After passing through the plant on Figure 4.5, or more precisely the left part of, the signal becomes y. Compared to θ, it is "turned upside down" because of the negative factor $(-b_1)$. Some constant is also added to it, but the y-axis is deliberately not shown.

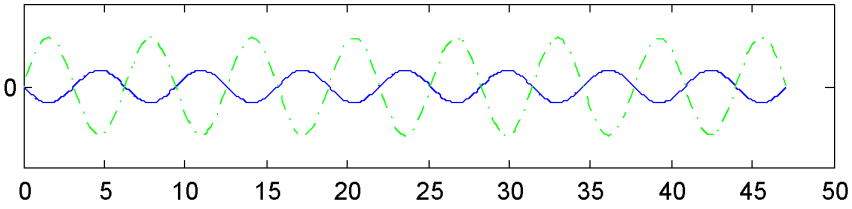

(c) The signal after passing through the high-pass filter $s/(s+h)$ from Figure 4.3. Signal $sin(\omega t)$ is also shown with green dashed line.

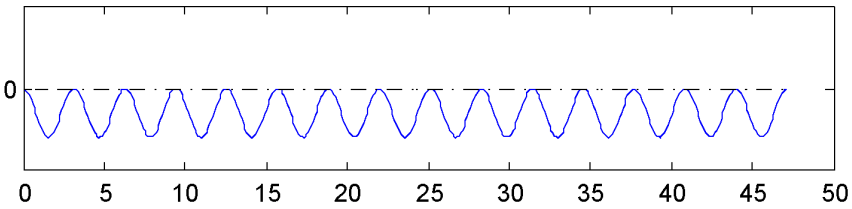

(d) Signal ξ from Figure 4.3, which is the product of the signals shown in (c). Since it is always negative, its integral multiplied with a negative constant will be a monotonically increasing function, which means that the signal $\hat{\theta}$ will increase, carrying $f(\theta)$ towards its minimum.

Figure 4.6: Signal propagation through the system for values of θ where $f(\theta) = a_1 - b_1\theta$.

- Finding the constant h in for the high-pass filter $s/(s+h)$ to dampen out constant components in plant output y quickly, while still letting the probing frequency ω through.
- Finding constant k for controller $-s/k$ high enough to allow quick convergence, but not so high as to make system unstable.

The scheme on Figure 4.8 introduces further details to the scheme on Figure 4.3. First, it has input dynamics $F_i(s)$ and output dynamics $F_o(s)$. Here, the advantage of using a harmonic probing signal comes into focus - since both of $F_i(s)$ and $F_o(s)$ are linear, their response to a harmonic signal $sin(\omega t)$ is a constant lag and multiplication by some factor. To cope with that, demodulation signal $sin(\omega t)$ is replaced with $sin(\omega t - \phi)$, where ϕ is the sum of the phase lag of input dynamics $F_i(s)$, output dynamic $F_o(s)$ and possibly also the washout filter $s/(s+h)$ if the latter has significant lag on the probing frequency.

Also, the minimum of the map f^* and the parameter θ^* are allowed to have dynamics described by

$$\mathcal{L}\{\theta^*(t)\} = \lambda_\theta \Gamma_\theta(s) \tag{4.4}$$

$$\mathcal{L}\{f^*(t)\} = \lambda_f \Gamma_f(s) \tag{4.5}$$

with known $\Gamma_\theta(s)$ and $\Gamma_f(s)$, but unknown - and possibly slowly varying - λ_θ and λ_f. The setup in Figure 4.3 us thus a special case of setup in Figure 4.8, with$\Gamma_\theta(s) = \Gamma_f(s) = 1/s$, $C_i(s) = k$ and $C_o(s) = 1/(s+h)$.

4.4.1 Mathematical proof

The rough analysis above by no means amounts to mathematical proof. The proof is also used for the investigation in the next section, Before the proof itself, a list of necessary conditions is presented, and certain variables are defined. The material presented in this section is copied from section 1.2 up till and including 1.2.1 in [1], with minimal additional commentary. Definitions from Figure 4.8 and Table 4.1 are used throughout this section.

Assumption 4.1. *$F_i(s)$ and $F_o(s)$ are asymptotically stable and proper*

Assumption 4.2. *$\Gamma_f(s)$ and $\Gamma_\theta(s)$ (as defined in (4.4), (4.5)) are strictly proper rational functions and poles of $\Gamma_\theta(s)$ that are not asymptotically stable are not zeros of $F_i(s)$.*

Assumption 4.3. *$\frac{C_o(s)}{\Gamma_f(s)}$ and $C_i(s)\Gamma_\theta(s)$ are proper.*

This assumption ensures that those filters are implementable. Since $C_i(s)$ and $C_o(s)$ are created by the designer, this assumption can always be satisfied.

Theorem 4.1 (Single Paraneter Extremum Seeking: LTV Test)**.** *For the system in Figure 4.8, under Assumptions 4.1, 4.2 and 4.3, the output error $\tilde{y}$ achieves local exponential convergence to an $\mathbb{O}(a^2)$ neighborhood of the origin provided $n = 0$ and:*

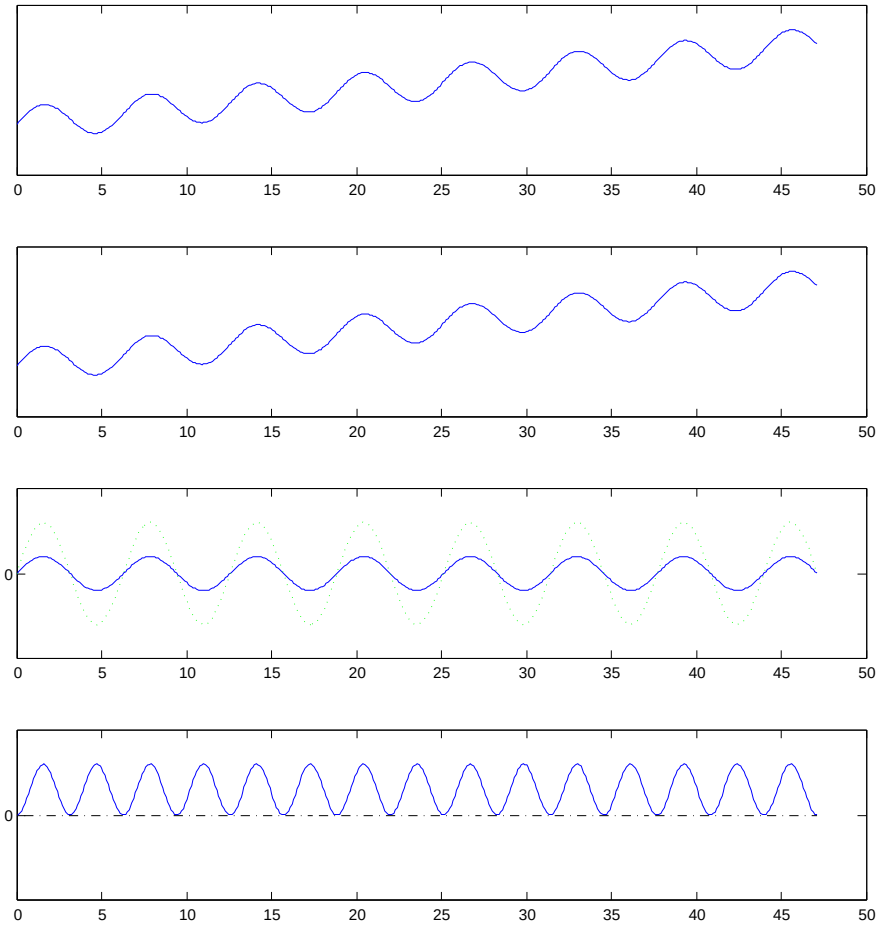

Figure 4.7: Signal propagation through the system for values of θ where $f(\theta) = a_2 + b_2\theta$. While on Figure 4.6 the output y from the plant and the demodulation signal $sin(\omega t)$ had *opposite phase*, here they are in *same phase*. This results in ξ being always positive in this figure, driving its negative integral $\hat{\theta} = -\int k\xi\, dt$ down, which is the right direction towards the minimum of $f(\theta)$, as shown on Figure 4.5.

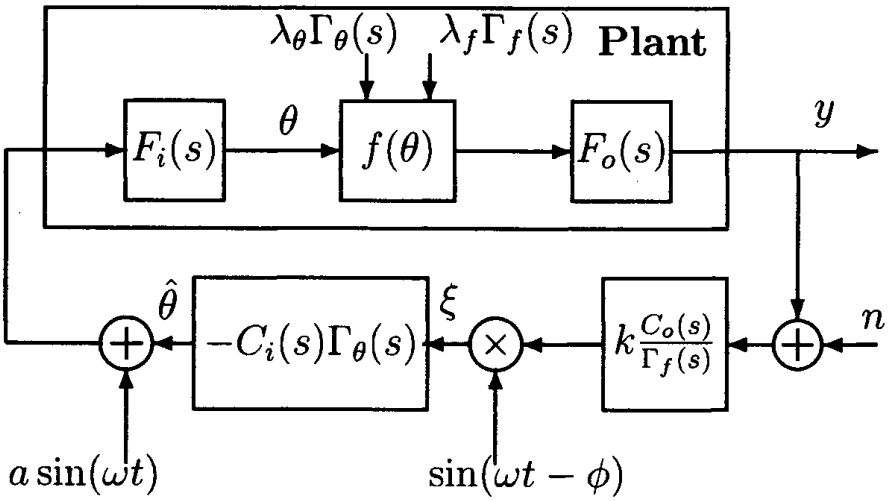

Figure 4.8: Full (linear SISO) Extremum Seeking scheme. Capable of handling input and output dynamics, dynamics in position of the extremum point as well lag of the plant on the probing frequency. Measurement noise n is also drawn, but will be set to zero in the proofs. The figure is a copy of Figure 1.2 in [1]

1. *$\pm j\omega$ is not a zero of $F_i(s)$.*
2. *Zeros of $\Gamma_f(s)$ that are not asymptotically stable are also zeros of $C_o(s)$.*
3. *Poles of $\Gamma_\theta(s)$ that are not asymptotically stable are not zeros of $C_i(s)$.*
4. *$C_o(s)$ is asymptotically stable and the eigenvalues of the matrix $\mathbf{\Phi}(T,0)$ lie inside the unit circle, where $T = 2\pi/\omega$ and $\Phi(T,0)$ is the solution at time T of the matrix differential equation*

$$\dot{\mathbf{\Phi}} = \dot{\mathbf{A}}(t)\mathbf{\Phi}(t,0), \quad \mathbf{\Phi}(0,0) = \mathbf{I},$$

and $\dot{\mathbf{x}} = \mathbf{A}(t)\,\mathbf{x}(t,0), \mathbf{x}(0) = \mathbf{x}_0$ is a state space representation of the LTV differential equation

$$den\{H_i(s)\}[\tilde{\theta}] = -f''\, num\{H_i(s)\}\left[sin(\omega t - \phi)H_0(s)[\theta_0(t)\tilde{\theta}]\right]$$

Proof. Setting $n = 0$ and substituting (4.7) and (4.10) in (4.9) yields

$$\tilde{\theta} = \theta^* + H_i(s)[\xi] \tag{4.15}$$

Further, substitution for ξ from (4.8) and for y from (4.6) yields

$$\tilde{\theta} = \theta^* + H_i(s)\left[sin(\omega t - \phi)H_o(s)\left[f^* + \frac{f''}{2}(\theta - \theta^*)^2\right]\right]. \tag{4.16}$$

Using $\theta - \theta^* = \theta_0 - \tilde{\theta}$ from (4.9), we get

Statements:

$$y = F_o(s)\left[f^*(t)\right] + \frac{f''}{2}(\theta - \theta^*(t))^2 \tag{4.6}$$

$$\theta = F_i(s)[asin(\omega t) - C_i(s)\Gamma_\theta(s)[\xi]] \tag{4.7}$$

$$\xi = k\, sin(\omega t - \phi)\frac{C_o(s)}{\Gamma_f(s)}[y + n] \tag{4.8}$$

Definitions:
Tracking error

$$\tilde{\theta} = \theta^*(t) - \theta + \theta_0 \tag{4.9}$$

$$\theta_0 = F_i(s)[asin(\omega t)] \tag{4.10}$$

Output error:

$$\tilde{y} = y - F_o(s)[f^*(t)] \tag{4.11}$$

$$H_i(s) = C_i(s)\Gamma_\theta(s)F_i(s) \tag{4.12}$$

$$H_o(s) \quad = \quad k\frac{C_o(s)}{\Gamma_f(s)}F_o(s) \tag{4.13}$$

$$y_2 = k\frac{C_o(s)}{\Gamma_f(s)}[y] = H_o(s)[f(\theta)] \tag{4.14}$$

Table 4.1: Statements and definitions necessary to prove Theorem 4.1

$$\begin{aligned}\tilde{\theta} &= \theta^* + H_i(s)\left[sin(\omega t - \phi)H_o(s)\left[f^* + \frac{f''}{2}(\theta_0 - \tilde{\theta})^2\right]\right] \\ &= \theta^* + H_i(s)\left[sin(\omega t - \phi)H_o(s)\left[f^* + \frac{f''}{2}\left(\theta_0^2 - 2\theta_0\tilde{\theta} + \tilde{\theta}^2\right)\right]\right]\end{aligned} \tag{4.17}$$

We drop the higher order term $\tilde{\theta}^2$(this is justified by Lyapunov's first method, as we have already written the system in terms of error variable $\tilde{\theta}$ thus transforming the problem to stability of the origin) and simplify the expression in (4.17) using Lemmas 6.1, 6.2 and assumptions 4.1, 4.2 and 4.3 and asymptotic stability of $C_o(s)/\Gamma_f(s)$ and $C_o(s)$:

$$\begin{aligned} sin(\omega t - \phi)H_o(s)[f^*(t)] &= \lambda_f sin(\omega t - \phi)\mathcal{L}^{-1}(H_o(s)\Gamma_f(s)) \\ &= sin(\omega t - \phi)(\epsilon^{-t}) \end{aligned} \tag{4.18}$$

$$sin(\omega t - \phi)H_o(s)\left[\theta_0^2\right] = C_1 a^2 sin(\omega t + \mu_1) + C_2 a^2 sin(3\omega t + \mu_2) + \epsilon^{-t} \tag{4.19}$$

where C_1, C_2, μ_1, $\mu_2$are constants (these can be determined from the frequency response of $H_o(s)$), and ϵ^{-t} denotes exponentially decaying terms. Now denote

$$u_{12}(t) = a^2 \frac{f''}{2}[C_1 sin(\omega t + \mu_1) + C_2 sin(3\omega t + \mu_2)]. \tag{4.20}$$

The tracking error equations, (4.17) after linearization (effected simply by dropping $\tilde{\theta}^2$ terms as we have expressed the system as an ODE in $\tilde{\theta}$) can be rewritten as

$$\tilde{\theta} = \theta^* + H_i(s)\left[u_{13}(t) + \epsilon^{-t} - f'' sin(\omega t - \phi)H_o(s)\left[\theta_0\tilde{\theta}\right]\right]. \tag{4.21}$$

Multiplying both sides of (4.21) with the denominator of $H_i(s)$, we get

$$den\left\{H_i(s)\right\}\left[\tilde{\theta}\right] = \epsilon^{-t} + num\left\{H_i(s)\right\}\left[u_{13}(t) + \epsilon^{-t} - f'' sin(\omega t - \phi)H_o(s)\left[\theta_0\tilde{\theta}\right]\right]. \tag{4.22}$$

The term θ^*drops out or becomes an exponentially decaying term when operated upon by $den\{\Gamma_\theta(s)\}$ contained in term $den\{H_i(s)\}$. We now write a state space representation of the LTV system in (4.22):

$$\dot{\mathbf{x}} = \mathbf{A}(t)\mathbf{x} + \mathbf{B}u_{13}(t), \quad \mathbf{A}(t+T) = \mathbf{A}(t),\ T = 2\pi/\omega. \tag{4.23}$$

The system has a state transition matrix $\mathbf{\Phi}(t, 0)$ given by the solution of

$$\dot{\mathbf{\Phi}} = \mathbf{A}(t)\mathbf{\Phi}(t, 0), \quad \mathbf{\Phi}(0, 0) = \mathbf{I} \tag{4.24}$$

The system is exponentially stable if the eigenvalues of the matrix $\mathbf{\Phi}(T, 0)$ (numerically calculated above) lie within the unit circle by Property 5.11 in [14]. As the persistent part of the non-homogeneous forcing term in (4.22) is $\mathbb{O}(a^2)$, we have convergence of $\tilde{\theta}$ to $\mathbb{O}(a^2)$, and therefore the convergence of $\tilde{y} = y - F_o(s)[f^*(t)] = F_o(s)\left[f''/2(\tilde{\theta} - \theta_0)^2\right]$ to $\mathbb{O}(a^2)$.

□

While the result above permits determination of stability of extremum seeking loops in a wide variety of classes, it is not a convenient *design* tool as it requires calculation of the state transition matrix of an LTV system. Such design tool is presented in section 1.2.2 of [1], and it is not intention of the present work to

repeat this section in its entirety. It is sufficient to say mention that tools that make it practical to design systems that satisfy conditions in Theorem 4.1 exist.

This system described in Figure 4.8 is very tolerant about the modeling errors. Nothing needs to be known about the plant except a rough estimate of input and output dynamics $F_i(s)$ and $F_o(s)$, and knowledge that function $f(\theta)$ has a minimum or a maximum (Figure 4.8 is searching for a minimum, to search for a maximum the filter $-C_i(s)\Gamma(s)$ has to be replaced with $+C_i(s)\Gamma(s)$).

However, if the phase lag on the probing frequency is not known exactly or is not constant, the ES process may become unstable if error becomes sufficiently large. In particular, if phase error reaches 180°, ES is guaranteed to move away from the extremum. Especially if the plant dynamics is of high order, phase lag on the probing frequency may be sensitive to changes in working parameters.

The technique presented in the next section is an addition to the Figure 4.8 that allows it to track the phase lag in input dynamics $F_i(s)$, which solves this problem for a large class of systems. The technique is particularly useful for systems which a time-variant (such as a cargo ship which is being offloaded), or there is variation between fabrication units.

4.5 Phase lag tracking

Phase lag tracking is a technique developed in this thesis. It can be used on a class of problems where lag of the probing frequency in the input dynamics $H_i(s)$ is either unknown or time-variant. This technique has its limitations: it is not GAS, it needs to be slow to allow exponentially decaying terms to settle, and it can do nothing to determine the lag of the output dynamics $H_o(s)$.

Possible areas of application are systems that are time-variant, for example a ship that is being offloaded, or if there is variation between manufacturing units.

Idea with multiplication with the second harmonic of the modulation frequency mentioned in [2], but neither proof nor an implementation suggestion provided.

The setup is an addition to extremum seeking scheme. The principal change compared to the standard ES setup is that demodulation factor $sin(\omega t - \phi)$ is replaced with $sin(\omega t - \hat{\phi})$, with $\hat{\phi}$ being the estimate of the phase lag on the modulation frequency.

4.5.1 Motivational analysis

The idea behind phase lag tracking is simple. Consider a system as described on Figure 4.8, but without output dynamic ($H_o(s) \equiv 1$) . Define $y_2 = k\frac{C_o(s)}{\Gamma_f(s)}$, and assume that $k\frac{C_o(j\bar{\omega})}{\Gamma_f(j\bar{\omega})} = 1$ for $\bar{\omega} > \omega$, with ω being the particular probing frequency and not frequency in general. It can be shown that if $y_2 = k\frac{C_o(s)}{\Gamma_f(s)}[y]$ is multiplied by signal $\kappa = cos(2\omega t - 2\hat{\phi})$, the low-frequency part of the product $p(\hat{\phi})$ will have its maximum when $\hat{\phi} = -\angle F_i(j\omega)$.

To find this maximum, the controller plays a kind of hide-and-seek game. It starts with an initial guess $\hat{\phi}$. To find which direction it should go, it compares values of $p(\hat{\phi}+\bar{\phi})$ and $p(\hat{\phi}-\bar{\phi})$. If $p(\hat{\phi}+\bar{\phi}) > p(\hat{\phi}-\bar{\phi})$, then $p(\hat{\phi}+\bar{\phi})$ is "warmer" than $p(\hat{\phi}-\bar{\phi})$, and $\hat{\phi}$ should increase. The situation is of course vice versa if $p(\hat{\phi}+\bar{\phi}) < p(\hat{\phi}-\bar{\phi})$, and $\hat{\phi}-\bar{\phi}$ would be closer to the maximum.

Interestingly, the first method to find the minimum of the function in (**??**) was to use another extremum seeking loop, with $\hat{\phi_b^-}$ as controlled variable and the expression in (**??**) as the function to be minimized. This solution was implemented and worked, but was eventually discarded for the solution described in Figure 4.9.

4.5.2 Lag tracking scheme

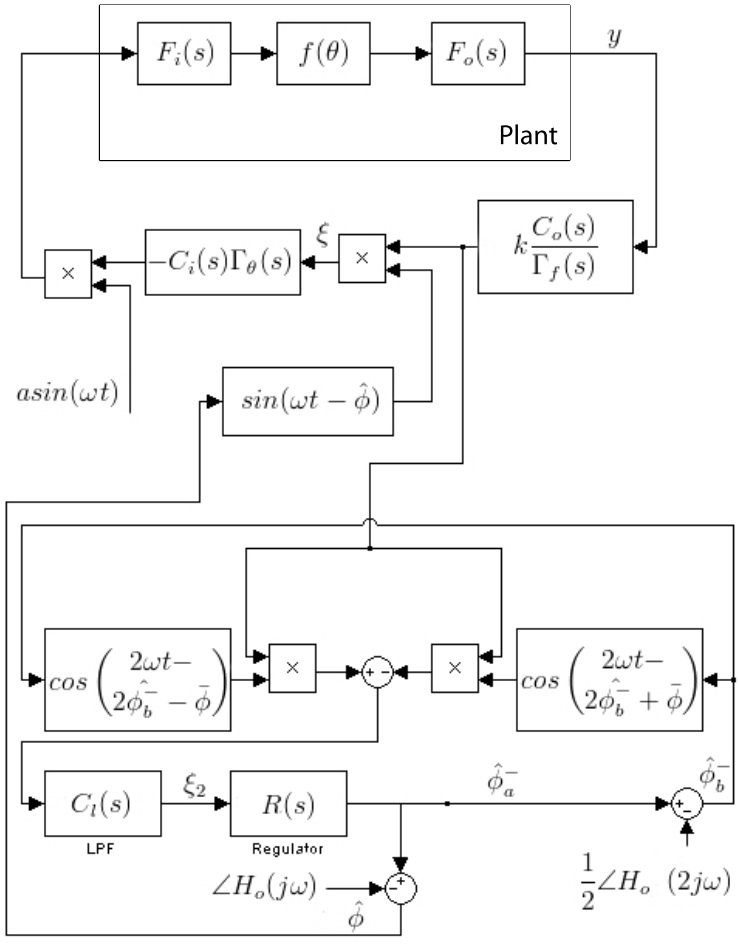

Figure 4.9: Extremum Seeking with modulation frequency lag tracking

4.5.3 Stability test

The first thing that needs to be shown is that the ES loop remains stable in presence of a small, non-constant error in phase lag estimate.

Theorem 4.2. *For the system on Figure 4.9, the output error $\tilde{y}$ achieves local exponential convergence to $\mathbb{O}(a^2)$ in presence of a phase lag estimation error $\tilde{\phi} = \phi - \hat{\phi}$ under the same assumptions as for the Theorem 4.1.*

Proof. An error in the estimate of the phase lag demodulation frequency means that the demodulation signal changes from $sin(\omega t - \phi)$ to $sin(\omega t - \phi + \tilde{\phi})$. To make the proof easier, the phase lag error is represented by changing the input to $asin(\omega t - \tilde{\phi})$ by applying time shift $t_{old} = t_{new} - \frac{\tilde{\phi}}{\omega}$. The rest of the proof closely follows proof of the Theorem 4.1. Compared to equations in Table 4.1 this time shift means that (4.7) changes to

$$\theta_{02} = F_i(s)\left[asin(\omega t - \tilde{\phi})\right] \tag{4.25}$$

Sub-index "2" is added to separate it from the original equation 4.10. Next, since $f^* = \Gamma_f(s)$, and $C_o(s)$ is asymptotically stable, $\mathcal{L}^{-1}\{H_o(s)[y^*]\} = \mathcal{L}^{-1}\{H_o(s)\Gamma_f(s)\} = \epsilon^{-t}$ and (4.18) holds. Examining if (4.19) holds as well:

$$\begin{aligned}
&sin(\omega t - \phi)H_o(s)\left[\theta_{02}^2\right] \\
=&sin(\omega t - \phi)H_o(s)\left[a^2 sin^2(\omega t - \tilde{\phi})\right] \\
=&a^2 sin(\omega t - \phi)H_o(s)\left[\frac{1 - cos(2\omega t - 2\tilde{\phi})}{2}\right] \\
=&a^2 sin(\omega t - \phi)\underbrace{H_o(s)\left[\frac{1}{2}\right]}_{\epsilon^{-t}} - \frac{1}{2}a^2 sin(\omega t - \phi)H_o(s)\left[cos\left(2\omega t - 2\tilde{\phi}\right)\right] \\
=&-\frac{1}{4}a^2|H_o(j2\omega)|\left(sin(3\omega t - 2\tilde{\phi} - \phi + \angle H_o(j2\omega)) - sin(\omega t - 2\tilde{\phi} + \phi + \angle H_o(j2\omega))\right) + \epsilon^{-t} \\
=&\frac{1}{4}|H_o(j2\omega)|a^2\left(sin(\omega t - 2\tilde{\phi} + \phi + \angle H_o(j2\omega)) - sin(3\omega t - 2\tilde{\phi} - \phi + \angle H_o(j2\omega))\right) + \epsilon^{-t}
\end{aligned} \tag{4.26}$$

Just as in Theorem 4.1, we define

$$u_{132}(t, \hat{\phi}) = \frac{1}{4}a^2\frac{f''}{2}|H_o(j2\omega)|\left(sin(\omega t - 2\tilde{\phi} + \phi + \angle H_o(j2\omega)) - sin(3\omega t - 2\tilde{\phi} - \phi + \angle H_o(j2\omega))\right) \tag{4.27}$$

and notice that $|u_{132}(t, \hat{\phi})| \leq \frac{1}{8}a^2 f''$ after the exponentially decaying terms ϵ^{-t} settle.

Continuing to follow the proof in Theorem 4.1, writing down the linearized form of equation (4.17), and multiplying both sides with the denominator of $H_i(s)$, get

$$den\{H_i(s)\}[\tilde{\theta}] = \epsilon^{-t} + num\{H_i(s)\}\left[u_{132}(t, \tilde{\phi}) + \epsilon^{-t} - f'' sin(\omega t - \phi)H_o(s)[\theta_{02}\tilde{\theta}]\right] \tag{4.28}$$

The difference between this and equation (4.22) is that variables θ_0 and u_{13} are replaced with θ_{02} and u_{132}. Looking at $\theta_{02}\tilde{\theta}$

$$\begin{aligned}\theta_{02}\tilde{\theta} &= asin(\omega t - \tilde{\phi})\tilde{\theta} \\ &= a\left(sin(\omega t)cos(\tilde{\phi}) - cos(\omega t)sin(\tilde{\phi})\right)\tilde{\theta}\end{aligned} \tag{4.29}$$

Since we are doing a local analysis, we can linearize by removing the second order term $sin(\tilde{\phi})\tilde{\theta}$, and set $cos(\tilde{\phi}) = 1$, yielding

$$\theta_{02}\tilde{\theta} \approx \theta_0\tilde{\theta} \tag{4.30}$$

with θ_0 being exactly as defined in Table 4.1. This transforms equation (4.28) to

$$den\{H_i(s)\}[\tilde{\theta}] = \epsilon^{-t} + num\{H_i(s)\}\left[u_{132}(t,\tilde{\phi}) + \epsilon^{-t} - f''sin(\omega t - \phi)H_o(s)[\theta_0\tilde{\theta}]\right] \tag{4.31}$$

Now, $-num\{H_i(s)\}\left[f''sin(\omega t - \phi)H_o(s)[\theta_0\tilde{\theta}]\right]$ is a periodic linear time-varying function of $\tilde{\theta}$ with θ_0 and $sin(\omega t - \phi)$ being the time-varying terms with period $T = 2\pi/\omega$. This means that (4.31) can be represented as a periodic LTV system

$$\dot{x} = A(t)x + Bu_{132}(t,\tilde{\phi}), A(t+T) = A(t), T = 2\pi/\omega \tag{4.32}$$

With A(t) being exactly the same as in equation in (4.23) and u_{132}, the persistent part of the forcing term, being $\mathbb{O}(a^2)$, and thus we have convergence of $\tilde{\theta}$ to $\mathbb{O}(a^2)$ and therefore also convergence of $\tilde{y} = y - F_o(s)[f^*(t)]$ to $\mathbb{O}(a^2)$ under the same conditions as in Theorem 4.1.

□

Assumption 4.4. *$\hat{\theta}$ is sufficiently dampened on frequencies ω and higher.*

This assumption means that modulation signal $asin(\omega t)$ dominates over $\hat{\theta}$ on frequency ω. This is not a very far far-fetched assumption since $\Gamma_\theta(s)$ is a low-pass filter.

Assumption 4.5. *$\angle F_o(2j\omega)$ is known.*

Since $k\frac{C_o(s)}{\Gamma_f(s)}$ is specified by designer and $H_o(s) = k\frac{C_o(s)}{\Gamma_f(s)}F_o(s)$, Assumption 4.5 implies that also $\angle H_o(2j\omega)$ is also known. This assumption is obviously quite limiting and it requires a good model of output dynamics. Of course, this is not limiting at all if there are no output dynamics, i.e. $F_o(s) \equiv 1$.

Notice that ω is in this context the particular probing frequency and not the frequency in general, so ~~$s = j\omega$~~ does not apply.

Theorem 4.3 (Vannsjø Theorem)**.** *The part of the system on figure 4.9 with $\tilde{\phi}$ as input and $-\xi_2$ as output is passive, with $\tilde{\phi} = -\angle F_i(j\omega) - \hat{\phi}_a^- = \phi - \hat{\phi}$ being the error in the estimate of the phase lag in the input dynamics on the probing frequency.*

ϕ	The total phase lag on the probing frequency of $F_i(s)$ and $H_o(s)$; $\phi = -\angle F_i(j\omega)H_o(j\omega)$
$\hat{\phi}$	Estimate of ϕ
$\hat{\phi_a^-}$	Estimate of phase lag of the plant input dynamics on the probing frequency, i.e. $-\angle F_i(j\omega)$
$\tilde{\phi}$	Error in the estimate $\hat{\phi}$. $\tilde{\phi} = \phi - \hat{\phi} = \phi_a^- - \hat{\phi_a^-}$

Table 4.2: Definitions of variables related to phase lag

Proof. Using definitions in Table 4.1, and in addition defining θ_i so that $\theta = F_i(s)[\theta_i]$ and $\hat{\tilde{\theta}} = F_i(s)[\hat{\theta}] - \theta^*$, and stating that $f(\theta) = f^* + \frac{f''}{2}\left(\theta - \theta^*(t)\right)^2$ in some neighborhood of $\theta^*(t)$ we get

$$\theta_i = \hat{\theta} + asin(\omega t)$$
$$\theta = F_i(s)[\hat{\theta}] + F_i(s)\left[asin(\omega t)\right] = \theta^* + \hat{\tilde{\theta}} + F_i(s)[asin(\omega t)]$$

Notice that the time shift from Theorem 4.2 is not used. Calculating $y_2 \triangleq k\frac{C_o(s)}{\Gamma_f(s)}[y]$:

$$\begin{aligned}
y_2 &= H_o(s)[f(\theta)] = H_o(s)\left[f^* + \frac{f''}{2}\left(\hat{\tilde{\theta}} + F_i(s)[a\,sin(\omega t)]\right)^2\right] \\
&= H_o(s) \\
&\cdot \left[f^* + \frac{f''}{2}\hat{\tilde{\theta}}^2 + \frac{f''}{2}F_i(s)[asin(\omega t)]F_i(s)[asin(\omega t)] + \frac{f''}{2}2\hat{\tilde{\theta}}F_i(s)[asin(\omega t)]\right] + \epsilon^{-t} \\
&= H_o(s)[f^*] + \frac{f''}{2}|F_i(j\omega)|^2a^2H_o(s)[sin^2\left(\omega t + \angle F_i(jw)\right)] \\
&+ f''\hat{\tilde{\theta}}H_0(s)F_i(s)[asin(\omega t)] + \frac{f''}{2}H_o(s)[\hat{\tilde{\theta}}^2] + \epsilon^{-t}
\end{aligned} \tag{4.33}$$

By substituting $sin^2(x) = \frac{1}{2}(1 - cos(2x))$, have

$$H_o(s)[sin^2\left(\omega t + \angle F_i(jw)\right)] = \underbrace{H_o(s)\left[\frac{1}{2}\right]}_{\epsilon^{-t}} - \frac{1}{2}H_o(s)[cos\left(2\omega t + 2\angle F_i(jw)\right)]$$
$$= -\frac{1}{2}|H_o(j2\omega)|cos\left(2\omega t + 2\angle F_i(jw) + \angle H_o(j2\omega)\right) + \epsilon^{-t}$$

This allows transforming (4.33) to

$$\begin{aligned}
y_2 &= H_o(s)[f^*] \\
&- \frac{f''}{4}|F_i(j\omega)|^2a^2|H_o(j2\omega)|cos\left(2\omega t + 2\angle F_i(jw) + \angle H_o(j2\omega)\right) + \\
&+ f''\hat{\tilde{\theta}}H_0(s)F_i(s)[asin(\omega t)] + \frac{f''}{2}H_o(s)[\hat{\tilde{\theta}}^2] + \epsilon^{-t}
\end{aligned} \tag{4.34}$$

Next, this signal is multiplied with

$$cos(2\omega t - 2\hat{\phi_b^-} - \bar{\phi}) - cos(2\omega t - 2\hat{\phi_b^-} + \bar{\phi}) \tag{4.35}$$

and put through low-pass filter $C_l(s)$ which dampens out frequencies from ω and higher, so that $C_l(0) = 1, C_l(j\bar{\omega}) \ll 1$ for $\bar{\omega} > \omega$. Only one term in (4.34) contains frequency 2ω. The other terms will become exponentially decaying when multiplied with (4.35) and then acted upon by $C_l(s)$. In particular $\hat{\tilde{\theta}}$ is sufficiently dampened on modulation frequency ω per Assumption 2 and is bounded per Theorem 4.2. Thus, after low-pass filtering, we have

$$\begin{aligned}
\xi_2 =& -\frac{f''}{4}|F_i(j\omega)|^2 a^2 |H_o(j2\omega)|\cdot \\
& \cdot C_l(s)[cos\left(2\omega t + 2\angle F_i(jw) + \angle H_o(j2\omega)\right) \\
& \left(cos(2\omega t - 2\hat{\phi_b^-} - \bar{\phi}) - cos(2\omega t - 2\hat{\phi_b^-} + \bar{\phi})\right)] + \epsilon^{-t} = \\
=& -\frac{f''}{4}|F_i(j\omega)|^2 a^2 |H_o(j2\omega)|\cdot \\
& \frac{1}{2}\cdot C_l(s)[cos(4\omega t + 2\angle F_i(jw) + \angle H_o(j2\omega) - 2\hat{\phi_b^-} - \bar{\phi}) - \\
& - cos(4\omega t + 2\angle F_i(jw) + \angle H_o(j2\omega) - 2\hat{\phi_b^-} + \bar{\phi}) + \\
& + cos(2\angle F_i(jw) + \angle H_o(j2\omega) + 2\hat{\phi_b^-} + \bar{\phi}) - \\
& - cos(2\angle F_i(jw) + \angle H_o(j2\omega) + 2\hat{\phi_b^-} - \bar{\phi})] + \epsilon^{-t}
\end{aligned} \tag{4.36}$$

$cos(a)\cdot cos(b) = \frac{1}{2}(cos(a-b) + cos(a+b))$

Again, $C_l(s)$ acting on parts of the sum with frequency 4ω, which - still assuming that $C_l(j\bar{\omega}) \ll 1$ for $\bar{\omega} = 4\omega$ - results in only exponentially decaying terms. Looking at the low-frequency part

$$\begin{aligned}
& cos(2\angle F_i(jw) + \angle H_o(j2\omega) + 2\hat{\phi_b^-} + \bar{\phi}) \\
-& cos(2\angle F_i(jw) + \angle H_o(j2\omega) + 2\hat{\phi_b^-} - \bar{\phi}) \\
=& cos(2\angle F_i(jw) + \angle H_o(j2\omega) + 2\hat{\phi_b^-} + \bar{\phi}) \\
+& cos(2\angle F_i(jw) + \angle H_o(j2\omega) + 2\hat{\phi_b^-} - \bar{\phi} + \pi) \\
=& 2cos\left(\frac{4\angle F_i(jw) + 2\angle H_o(j2\omega) + 4\hat{\phi_b^-} + \pi}{2}\right) cos\left(\frac{2\bar{\phi} - \pi}{2}\right) \\
=& -2\underbrace{sin(\bar{\phi})}_{constant} sin\left(2\angle F_i(jw) + \angle H_o(j2\omega) + 2\hat{\phi_b^-}\right)
\end{aligned} \tag{4.37}$$

Substituting the above into (4.36), we get

$$\begin{aligned}
\xi_2 =& -\frac{f''}{4}|F_i(j\omega)|^2 a^2 |H_o(j2\omega)|\frac{1}{2}C_l(s) \\
& \left[-2sin(\bar{\phi})sin\left(2\angle F_i(jw) + \angle H_o(j2\omega) + 2\hat{\phi_b^-}\right)\right] + \epsilon^{-t} = \\
=& \frac{f''}{4}|F_i(j\omega)|^2 a^2 |H_o(j2\omega)|sin(\bar{\phi})|C_l(0)|sin(\bar{\phi})\cdot \\
& \cdot sin\left(2\angle F_i(jw) + \angle H_o(j2\omega) + \angle C_l(0) + 2\hat{\phi_b^-}\right) + \epsilon^{-t}
\end{aligned} \tag{4.38}$$

Substituting $\hat{\phi_b^-} = \hat{\phi_a^-} - \frac{1}{2}\angle H_o(j2\omega)$ and $C_l(0) = 1$,

$$\xi_2 = \frac{f''}{4}|F_i(j\omega)|^2 a^2 |H_o(j2\omega)| sin(\bar{\phi}) sin\left(2\angle F_i(jw) + 2\hat{\phi_a^-}\right) + \epsilon^{-t} \tag{4.39}$$

Next, since $\tilde{\phi} = -\angle F_i(j\omega) - \hat{\phi_a^-}$ have [1]

$$\xi_2 = \frac{f''}{4}|F_i(j\omega)|^2 a^2 |H_o(j2\omega)| sin(\bar{\phi}) sin\left(-2\tilde{\phi}\right) + \epsilon^{-t} \tag{4.40}$$

Discarding the exponentially decaying tern ϵ^{-t}, we have

$$-\xi_2\tilde{\phi} \geq 0 \ , \ \tilde{\phi} \in [-\pi/2, \pi/2] \tag{4.41}$$

The part of system with $\tilde{\phi}$ as input and $-\xi_2$ as output is passive. Any passive controller can be used as regulator $R(s)$, as long as it is slow enough to allow the exponentially decaying terms to settle.

□

Corollary 4.4. *Controller $\hat{\phi}_a^- = -\frac{k_1}{s}[\xi_2] - k_2\xi_2$ is passive with ξ_2 as input and $\tilde{\phi}$ as output for any $k_1, k_2 \in \mathbb{R}^+$.*

Proof. Substituting

$$\tilde{\phi} = -\angle F_i(j\omega) - \hat{\phi}_a^- = -\angle F_i(j\omega) + \frac{k_1}{s}[\xi_2] + k_2\xi_2 \tag{4.42}$$

and defining a positive semi-definite storage function V per relationship

$$2k_1 V = \left(\frac{k_1}{s}[\xi_2] - \angle F_i(j\omega)\right)^2 \tag{4.43}$$

Then, assuming that $\frac{d}{dt}\angle F_i(j\omega)$ is negligible have

$$\dot{V} = \left(\frac{k_1}{s}[\xi_2] - \angle F_i(j\omega)\right)\xi_2 \tag{4.44}$$

Substituting for $\frac{k_1}{s}[\xi_2]$ from (4.42),

$$\dot{V} = (\tilde{\phi} - k_2\xi_2)\xi_2 \leq \tilde{\phi}\xi_2 \tag{4.45}$$

□

Thus, the scheme on figure (**??**) with $R(s) = \frac{k_1}{s} + k_2\xi_2$ is an interconnection of two passive systems (with one negative connection because passivity in theorem 4.3 is proven for $-\xi_2$ as output. The entire system is therefore passive and since it is unforced it is also stable.

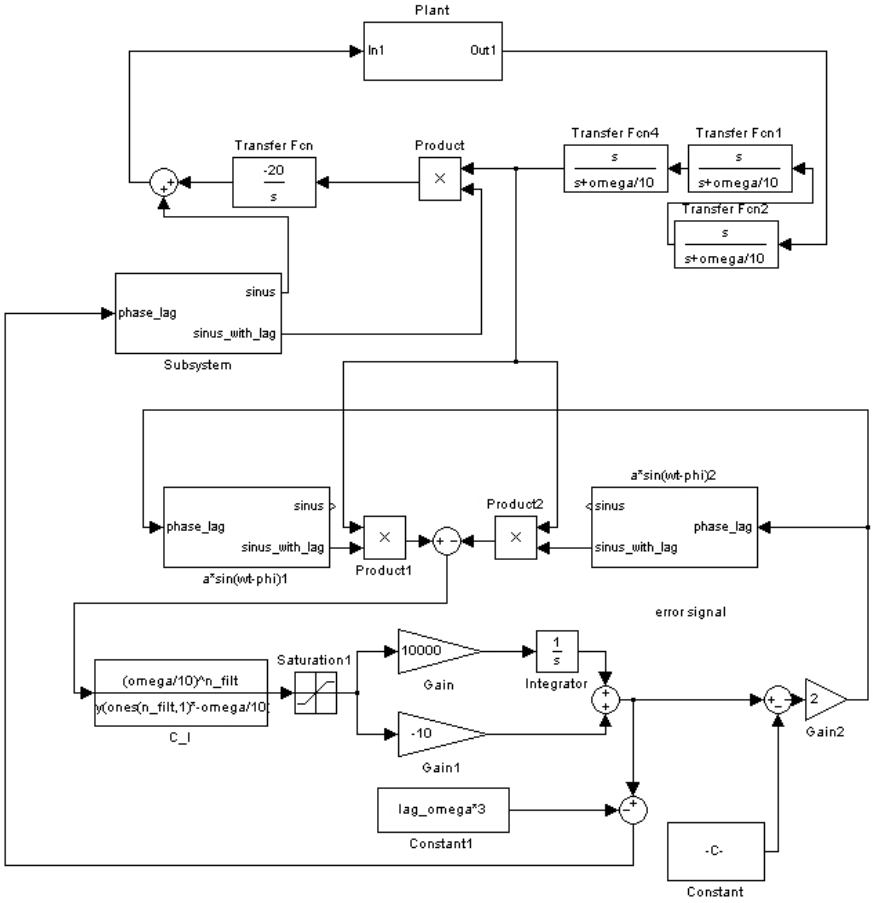

Figure 4.10: Simulink implementation of optimal direction controller

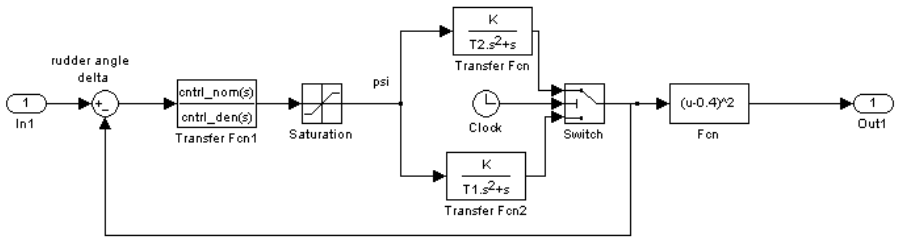

Figure 4.11: Contents of the Plant box on Figure 4.10

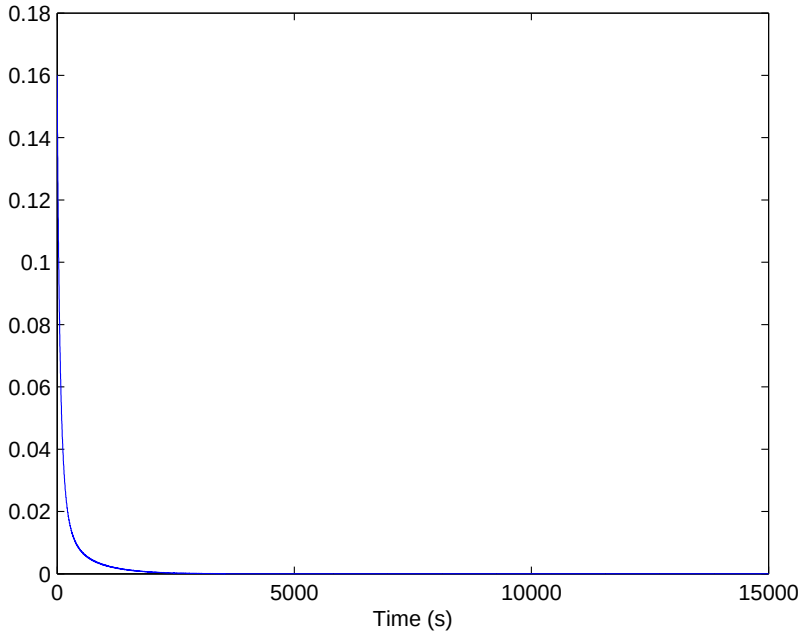

Figure 4.12: Cost function

4.6 Applying Extremum Seeking to this model

Implementation of controller locating the otimal direction for the system is shown on Figure 4.10. Contents of the Plant box are shown on Figure 4.11. The implementation follows the scheme on Figure 4.9, with exception of a saturaion element in regulator R. Due to implementational concern, instead of continuous transition the model of the ship changes its time constant T to 213.6s at simulation time 8000s. The probing frequency $\omega = 0.5$s was selected, giving probing period of $T = 2\pi/\omega = 12$s. This is high enough frequency to allow quick convergence, but could lead to intereference with waves if they will be included in the model.

The main difficulty encountered is that the system is that exponentially decaying terms from Theorem 4.3 can take too long time to decay. For that reason, high-order filters are employed as both as $C_o(s)$ and $C_l(s)$. Also, a saturation element after $C_l(s)$ limits the effects of the disturbance until the exponentially decaying terms settle.

4.7 Results

The results of simulation are shown in Figures 4.13-4.15. The controller successfully converges the cost function towards its minimum, which is zero. The lag

[1] Think of $\hat{\phi_a^-}$ as an estimate of $-\angle F_i(j\omega)$

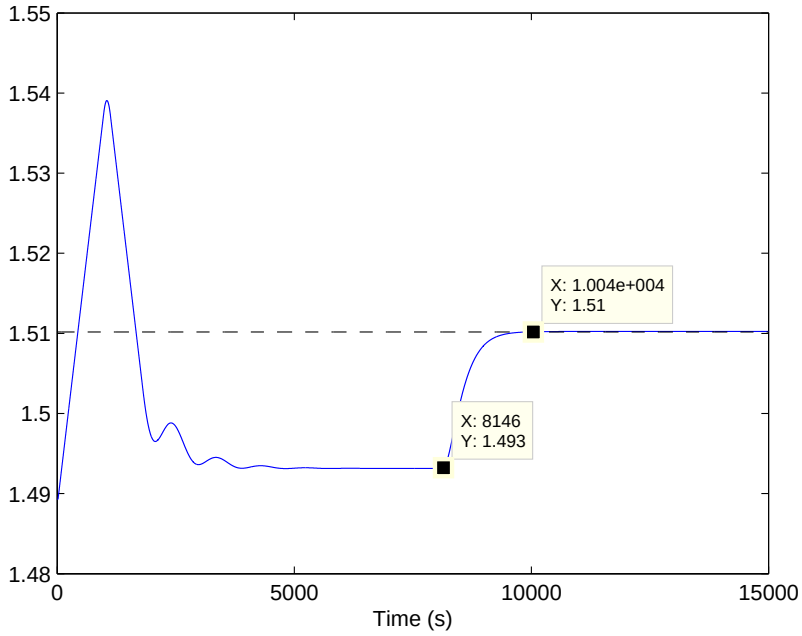

Figure 4.13: Estimate of lag, before and after the system changes. Theoretical value is shown with black dashed line, estimate is given with the blue line.

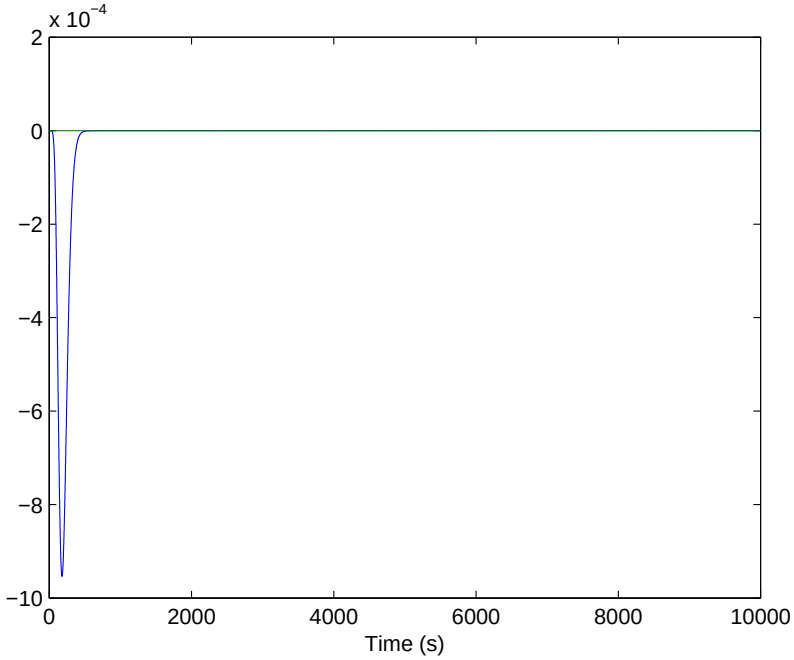

Figure 4.14: Error signal ξ_2. Large transients are observed before the exponentially decaying terms settle

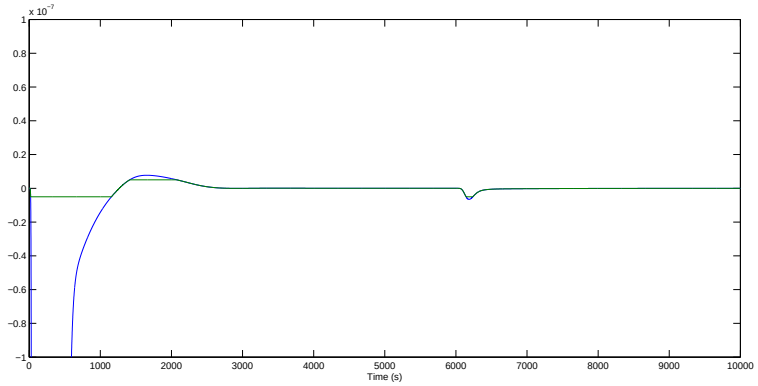

Figure 4.15: Figure 4.14 magnified. Effects of the saturation element are clearly seen.

on the modulation frequency can was calculated using the Control System toolbox as well, by adding frequency responses of plant input dynamics and $H_o(s)$. The code is shown in Algorithm 4.2. The calculated lag of the mutated system is shown on Figure 4.13 as a black dashed line. It shows that the value found using the method described in this work converges towards the value calculated with Control System Toolbox.

It is worth commenting that the phase estimation error converges after about 700 seconds, while the main extremum seeking loop converges only about 1500 seconds. This confirms the results from the theory, that phase lag tracking does not need $\tilde{\theta}$ to be close to zero in order to work.

4.8 Conclusion

In this chapter, possibility of doing the transfer operation on an optimal angle into the wave fronts using extremum seeking was considered. To allow the model to change underway, a modification of the Extremum Seeking scheme was made to allow it to cope with continuous changes in model parameters. This allows use of probing frequencies that can change significantly during an operation.

Algorithm 4.2 Calculating frequency response of $H_i(s)$ and $H_o(s)$

```
function w = getOmega()
omega = 0.5;
K = 0.185;
T = 107.3*2;
nom = [K];
den = [T, 1, 0];
sys = tf(nom, den);

K_p = 0.1; T_d = 14;
cntrl_nom = [T_d + K_p, K_p];
cntrl_den = [1 2];
cntrl = tf(cntrl_nom,cntrl_den);
H_o1 = tf([1 0],[1 omega/10]);

close_loop = cntrl* sys / (1+cntrl *sys);
sys_lag = freqresp(close_loop, omega);
H_o_lag = freqresp(H_o, omega)*3; % Three H_o's in series
w = sys_lag + H_o_lag;
```

Chapter 5

Conclusion

This thesis contains two different approaches to solve the same practical problem of transforming heavy equipment in heavy seas. Both approaches yielded some results. Chapter 3 proposes attaching fins to the sides of the smaller craft, and achieves sufficient improvement in stability. Chapter 4 yields interesting theoretical results. It has been shown that the proposed scheme can in fact handle sudden changes in the plant, but further testing is necessary to demonstrate applicability of this technique.

Chapter 6

Appendixes

6.1 Frequency response lemmas

Lemma 6.1. *If the transfer function $H(s)$ has all of its poles with negative real parts, then for any real ψ,*

$$H(s)[sin(\omega t - \psi)] = \mathbf{Im}\left\{H(j\omega)e^{j(\omega t-\psi)}\right\} + \epsilon^{-t},$$

where ϵ^{-t} denotes exponentially decaying terms.

This is simply the frequency response of an asymptotically stable LTI system.

Lemma 6.2. *For any two rational function $A(\cdot)$ and $B(\cdot,\cdot)$, the following is true:*

$$\begin{aligned}&\mathbf{Im}\left\{e^{j(\omega_a t-\psi)}A(j\omega_a)\right\} Im\left\{e^{j(\omega_b t-\phi)}B(s,j\omega_b)[z(t)]\right\}\\ =&\frac{1}{2}Re\left\{e^{j((\omega_b-\omega_a)t+\psi-\phi)}A(-j\omega_a)B(s,j\omega_b)[z(t)]\right\}\\ -&\frac{1}{2}Re\left\{e^{j((\omega_b+\omega_a)t-\psi-\phi)}A(+j\omega_a)B(s,j\omega_b)[z(t)]\right\}.\end{aligned}$$

Proof. Follows by substituting the representations for the real and imaginary parts of a complex number z, $Rez = \frac{z+\bar{z}}{2}$, and $Imz = \frac{z-\bar{z}}{2}$.

□

6.2 Contents of the attached DVD

Name	Type	Description

Name	Type	Description
waves_comp	Folder	Folder containing simulation of the system in bow-to-stern configuration as described in Chapter 3.
waves_comp/init.m	Matlab script	Initializes variables for the simulation.
waves_comp/Seabase.mdl	Simulink model	Simulink model.
actuation.avi	Video, cinepak	Animation of fin-acutated system.
no_actuation.avi	Video, cinepak	Animation of the same system as in actuation.avi, with fins inactive. Notice large angular movements of the ramp.
direction	Folder	Folder containing simulation in side-to-side configuration.
direction/init.m	Matlab script	Initializes variables before the simulation.
direction/autolag.mdl	Simulink model	Simulink model
direction/getOmega.m	Matlab script	Algorithm 4.2
direction/sinus_with_lag.mdl	Simulink library function	Simulink block for a sinus with variable phase. Add $\pi/2$ to the to the phase to get a cosine.
ControlFinal.pdf	PDF document/presentation	Presentation given by Professor Miroslav Krstić to ONR.

Bibliography

[1] K. B. Ariyur and M. Krstić, *Real-Time Optimization by Extremum-Seeking Control*, Wiley-Interscience, 2003

[2] A. G. Ivahrenko, P. I. Chinaev, N. M. Chumakov, V. I. Vasilyev, I. I. Vaisberg, S. F. Kozubovskij, V. I. Kostyuk *et al*, *Self-Tuning Systems, Spravochnik* , Naukova Duma, Kiev, 1968

[3] Frank M. White, *Fluid Mechanics*, McGraw Hill, 2003.

[4] John J. Bertin, *Aerodynamics for Engineers*, Prentice Hall, 2002

[5] Odd M. Faltinsen, *Hydrodynamics of High-Speed Marine Vehicles*, Cambridge University Press, 2006

[6] Thor Inge Fossen, *Marine Control Systems*, Tapir Trykkeri, Trondheim, 2002

[7] Claes Johnson and Johan Hoffman, "Why is it possible to fly", Google Knol, accessed on April 28th 2009, <http://knol.google.com/k/claes-johnson/why-it-is-possible-to-fly>. The authors claim to be Claes Johnson, professor of applied mathematics at the Royal Institute of Technology, Stockholm, Sweden and Johan Hoffman, an associate professor in numerical analysis at the Royal Institute of Technology KTH. Their identities could not be verified, source used with caution.

[8] J.Hoffman and C.Johnson, Finally: Resolution of d'Alembert's Paradox, *J. Math. Fluid Mech,* 2008.

[9] E. Kyrkjebø and K. Pettersen, "Leader-follower dynamic synchronization of surface vessels," in Proc. 7th IFAC Conf. on Manoeuvring and Control of Marine Craft, Lisboa, Portugal, September 2006.

[10] E. Børhaug, A. Pavlov, E. Panteley and K. Y. Pettersen, *Straight line path following for formations of underactuated marine surface vessels.* Submitted to IEEE Trans. Control Systems Technology, 2008.

[11] Various Wikibooks contributors, Wikibooks, *LaTeX/Floats, Figures and Captions*, <http://en.wikibooks.org/wiki/LaTeX/Floats,_Figures_and_Captions>.

[12] Goldstein, Poole and Safko, *Classical Mechanics*, 3rd edition, Addison Wesley.

[13] Iver H. Brevik, "Classical Mechanics, compendium in course TEP4145 Classical Mechanics" (orig. title "Klassisk Mekanikk, kompendium i faget TEP414", 2006. Available online as pdf at <http://www.ivt.ntnu.no/ept/fag/tep4145/klassisk_mekanikk.pdf>

[14] W. J. Rugh, *LinearSystemTheory*, Prentice Hall, Upper Saddle River, NJ, 1996.